Atmos. Chem. Phys. Discuss., https://doi.org/10.5194/acp-2019-43
Manuscript under review for journal Atmos. Chem. Phys.
Discussion started: 30 January 2019
© Author(s) 2019. CC BY 4.0 License.

Atmospheric Chemistry and Physics Discussions

Above Cloud Aerosol Optical Depth from airborne observations in the South-East Atlantic

Samuel E. LeBlanc[1,2], Jens Redemann[3], Connor Flynn[4], Kristina Pistone[1,2], Meloë Kacenelenbogen[1,2], Michal Segal-Rosenheimer[1,2] ,Yohei Shinozuka[1,2], Stephen Dunagan[2], Robert P. Dahlgren[5,2], Kerry Meyer[6], James Podolske[2], Steven G. Howell[7], Steffen Freitag[7], Jennifer Small-Griswold[7], Brent Holben[6], Michael Diamond[8], Paola Formenti[9], Stuart Piketh[10], Gillian Maggs-Kölling[11], Monja Gerber[11], Andreas Namwoonde[12]

[1]Bay Area Environmental Research Institute, Moffett Field, CA
[2]NASA Ames Research Center, Moffett Field, CA
[3]University of Oklahoma, Norman, OK
[4]Pacific Northwest National Laboratory, Richland, WA
[5]California State University Monterey Bay, Seaside, CA
[6]NASA Goddard Space Flight Center, Greenbelt, MD
[7]University of Hawai`i at Mānoa, Honolulu, HI
[8]University of Washington, Seattle, WA
[9]LISA, UMR CNRS 7583, Université Paris Est Créteil et Université Paris Diderot, Institut Pierre Simon Laplace, Créteil, France
[10]NorthWest University, South Africa
[11]Gobabeb Research and Training Center, Gobabeb, Namibia
[12]Sam Nujoma Marine and Coastal Resources Research Centre (SANUMARC), University of Namibia, Henties Bay, Namibia

Correspondence to: Samuel E. LeBlanc (samuel.leblanc@nasa.gov)

Abstract

The South-East Atlantic (SEA) is host to a climatologically significant biomass burning aerosol layer overlying marine stratocumulus. We present directly measured Above Cloud Aerosol Optical Depth (ACAOD) from the recent ObseRvations of Aerosols above CLouds and their intEractionS (ORACLES) airborne field campaign during August and September 2016. In our analysis, we use data from the Spectrometers for Sky-Scanning Sun-Tracking Atmospheric Research (4STAR) instrument and found an average ACAOD of 0.32 at 501 nm, with an average Ångström exponent (AE) of 1.71. The AE is much lower at 1.25 for the full column (including below cloud level aerosol), indicating the presence of large aerosol particles, likely marine aerosol, embedded within the vertical column. ACAOD is observed to be highest near coast at about 12°S, whereas its variability is largest at the southern edge of the average aerosol plume, as indicated by 12 years of MODIS observations. In comparison to MODIS derived ACAOD and long term fine-mode plume-average AOD, the directly-measured ACAOD from 4STAR is slightly lower than the ACAOD product from MODIS. The peak ACAOD expected from long term retrievals is measured to be closer to coast in 2016 at about 1.5° - 4°

Atmos. Chem. Phys. Discuss., https://doi.org/10.5194/acp-2019-43
Manuscript under review for journal Atmos. Chem. Phys.
Discussion started: 30 January 2019
© Author(s) 2019. CC BY 4.0 License.

Atmospheric Chemistry and Physics Discussions

W. By spatially binning the sampled AOD, we obtain a mean ACAOD of 0.37 for the SEA region. Vertical profiles of AOD showcase the variability of the altitude of the aerosol plume and its separation from cloud top. We measured larger AOD at high altitude near coast than farther from coast, while generally observing a larger vertical gap further from coast. Changes of AOD with altitude are correlated with a gas tracer of the biomass burning aerosol plume. Vertical extent of gaps between aerosol and cloud show a large distribution of extent, dominated by near zero gap. The gap distribution with longitude is observed to be largest at about 7°W, farther from coast than expected.

1 Introduction

Aerosol above clouds have been identified as a leading source of uncertainty in measuring the global source of aerosol burden, constituting globally 25±6% of total burden (Waquet et al., 2013a). In the South-East Atlantic (SEA), where one of the Earth's semi-permanent stratocumulus cloud decks exists, the frequency of occurrence of an overlying aerosol layer averaged over the entire region is more than 30% on an annual basis, and increase to more than 50% during the peak biomass burning season of July through November (Devasthale and Thomas, 2011, Zhang et al., 2016). These aerosols above clouds impact climate by either directly affecting the radiative budget (e.g., Schulz et al., 2006), by interacting with clouds via a change in the atmospheric thermal profile (semi-direct effects) (Sakaeda et al., 2011), or by directly modifying cloud properties (indirect/Twomey effect) (Bond et al., 2013; Twomey, 1974). One of the driving uncertainties in quantifying the impact of these aerosol is due to the difficulty in retrieving the Above Cloud Aerosol Optical Depth (ACAOD) from satellite measurements. Where the ACAOD is the Optical Depth of the aerosol layers that are present at higher altitudes than the cloud tops. To constrain the climatic effect of the aerosol above cloud in the SEA, an airborne field campaign, ObseRvations of Aerosols above CLouds and their intEractionS (ORACLES), was conducted in the peak of the biomass burning season (ORACLES Science Team, 2017). We show in this paper the directly measured ACAOD and its vertical dependence during the first phase of ORACLES.

Although much progress to quantify aerosols above clouds has been made, direct measurements of the ACAOD in the SEA is limited. Previous measurements during the Southern African Regional Science Initiative Project (SAFARI-2000) sampled only small, near coast portions of the overlying aerosol layer with limited instrumentation (Keil and Haywood, 2003; Bergstrom et al., 2003). To date, several passive satellite sensors (e.g., Moderate Resolution Imaging Spectroradiometer [MODIS], Polarization and Directionality of Earth's Reflectances [POLDER], Ozone Monitoring Instrument [OMI]) have been used to detect aerosol above clouds and retrieve ACAOD over the SEA region (e.g., Jethva et al (2013, 2014), Waquet et al. (2009, 2013b), Torres et al. (2012), De Graaf et al. (2012, 2014), Meyer et al. (2015), Peers et al. (2015), Feng and Christopher (2015), Sayer et al. (2016), Chang and Christopher (2016, 2017)). However, current passive satellite ACAOD retrieval techniques could be biased by what is called the "cloud adjacency effect" or the "3-D cloud radiative effect", i.e., brightening of cloud-free air near clouds (Wen et al., 2007). This is why some studies have used the active CALIOP (Cloud Aerosol LIdar with Orthogonal Polarization) instead of passive satellite sensors

© Author(s) 2019. CC BY 4.0 License.

to retrieve ACAOD (e.g. Chand et al., 2009; Wilcox, 2012; Matus et al., 2015; Zhang et al., 2014; Kacenelenbogen et al., in preparation). We refer the reader to Table 1 of Kacenelenbogen et al. (in preparation) for a more complete list of passive and active satellite sensors used in the observation of ACAOD over other parts of the world.

Not only is the climatological magnitude of the ACAOD in question, but its vertical dependence and relative distribution with respect to clouds are uncertain as well. Hobbs (2003) showed some first sampling of distinct Clear-Air-Slots (CAS) separating aerosol and cloud layers. A separation of the cloud and aerosol layers indicates that aerosols are not directly modifying cloud microphysical properties (e.g., Twomey 1977), but rather directly modify the radiation field and semi-directly the underlying clouds (e.g., Graßl, 1979, Lohmann and Feichter, 2005). Past work has shown that the elevated aerosol layers in this region are frequently separated from the underlying cloud top, e.g., Devasthale and Thomas (2011) found that 90-95% of above-cloud-aerosol cases observed by an active remote sensor (which has known limitations (Kacenelenbogen et al., 2014)) showing a gap extent larger than 100 m. Rajapakshe et al (2017) showed ~40% incidence of a gap between cloud top and aerosol layer bottom as measured by the spaceborne lidar Cloud-Aerosol Transport System (CATS; McGill et al., 2015), of which 60% have a gap of less than 360 m. Additionally, the gap extent is expected to be dependent on the distance from coast, decreasing further from coast, with few examples of situations without a gap between cloud and aerosol, as observed by CALIOP (Sakaeda et al., 2011; Wood et al., In prep).

In Section 2, we present an overview of the ORACLES first deployment and introduce the instruments and related data quality. Section 3 presents the measured ACAOD; their spatial and spectral dependence; and a comparison of the ACAOD to climatologies derived from MODIS satellite measurements. Additionally, in Section 3 we show some advanced analysis from the airborne sunphotometer with the vertical dependence of ACAOD and the measured gap between the aerosol layer and the clouds. The summary of our results is presented in Section 4. An appendix describes the data quality of the 4STAR instrument.

2 Data and instrumentation

We focus on the measured Aerosol Optical Depth (AOD) collected by the Spectrometers for Sky-Scanning Sun-Tracking Atmospheric Research (4STAR; Dunagan et al., 2013) airborne sunphotometer on board the NASA P-3 during ORACLES 2016. To better understand the overall observed scenes, we use information obtained from a combination of in situ instrumentations describing aerosol optical properties, cloud particles, and trace gas measurements. We also use nearby AERONET (Aerosol Robotic Network; Holben et al., 1998, 2018) stations, and regional satellite AOD data for spatial context and comparisons. Satellite measurements give context by either a long-term record using neighboring clear sky AOD retrieval from the Moderate resolution Imaging Spectroradiometer (MODIS; Levy et al., 2013) or a short-term record using the newly developed retrieval of ACAOD from MODIS (Meyer et al., 2015).

© Author(s) 2019. CC BY 4.0 License.

2.1 ObseRvations of Aerosols above CLouds and their intEractionS (ORACLES)

The ORACLES field campaign is aimed at directly measuring the SEA ACAOD via airborne sampling during 3 intensive operating periods (Sep 2016, Aug 2017, Oct 2018) (Zuidema et al., 2016). We use the NASA P-3 as an airborne platform for in situ and remote sensing measurements of aerosols and clouds in three campaigns, and the NASA ER-2 high altitude remote sensing platform in year 2016. The first deployment out of Walvis Bay, Namibia, was successfully completed from 27 August to 29 September 2016 with 15 research flights for the P-3 (ORACLES Science Team, 2017). Nearly half of these research flights followed a routine flight path extending diagonally from 13°E, 23°S to 0°E, 10°S and the other half focused on paths with increased chance of successful sampling with all instruments (see Fig. 1). All flights (P-3 and ER-2) were planned using the flight planning software developed by LeBlanc (2018).

2.2 Spectrometers for Sky-Scanning Sun-Tracking Atmospheric Research (4STAR)

4STAR (Dunagan et al., 2013) combines airborne sun tracking and sky scanning with diffraction spectroscopy. This airborne sun tracker and sky radiometer has multiple operating modes, which are selected by an operator depending on the sky conditions. In this paper, we present results from 4STAR's direct solar beam irradiance measurements; when 4STAR is in the sunphotometer mode. The hyperspectral measurements of 4STAR enable continuous AOD spectrum measurements, broken only by gas absorption lines, where the aerosol extinction has smoothly varying spectral features (e.g., Dunagan et al., 2013). 4STAR incorporates a modular sun-tracking/sky-scanning optical head with fiber optic signal transmission to rack-mounted spectrometers. Using 2 spectrometers, 4STAR samples light with wavelengths ranging from 350 nm to 1750 nm, with sampling resolution of 0.2 - 1 nm below 1000 nm and 3 - 6 nm at longer wavelengths. The full width of the field of view for the direct beam irradiance measurement is 2.4° with radiometric deviations of less than 1% across this span. The nominal calibration accuracy of AOD measurements from 4STAR are dependent on wavelength, time of day, tracking stability, and various corrections (such as removal of light absorption by trace gases). This accuracy is typically near 1% in transmittance resulting in an AOD uncertainty of 0.01 at solar noon. The details on the corrections and calibrations of 4STAR are found in the appendix.

2.3 In situ instrumentation: HiGEAR, PDI, and COMA

A combination of in situ instruments is used to provide context of the AOD measurements. We use aerosol scattering from nephelometers from the Hawaii Group for Environmental Aerosol Research (HiGEAR), cloud number concentration from the Artium Flight Probe Dual Range Phase Doppler Interferometer (PDI), and CO concentration from CO Measurements and Analysis (COMA), as described below.

We used nephelometers as part of the HiGEAR extensive airborne measurement suite to quantify the aerosol scattering coefficient (similar to Howell et al. 2006). These nephelometers directly ingest aerosol from ambient air, together with other HiGEAR instrumentation provide size resolved assessment of aerosol physical and chemical properties and their relationship to measured optical and microphysical behavior. The scattering coefficient of the aerosol is sampled with 3-wavelength nephelometers (TSI 3563, at 450 nm, 550 nm, and 700 nm) while

© Author(s) 2019. CC BY 4.0 License.

dependence on humidity is measured with paired single-wavelength nephelometers (Radiance Research M903 measuring at 540 nm, with air in one humidified to 80% relative humidity while RH in the other was uncontrolled). Comparisons between the dry Radiance Research to the TSI nephelometers are used to correct the Radiance Research truncation issues, while the humidity dependence of the scattering coefficient is calculated from a gamma relationship obtained from the paired Radiance Research nephelometers (following Quinn et al., 2005). The absorption coefficient used to create a combined extinction coefficient is measured in dry conditions using Particle Soot Absorption Photometers (PSAP) from Radiance Research. The solid diffuser inlet efficiently samples particles <1µm, with a 50% cutoff at approximately 3 µm (McNaughton et al., 2007).

Cloud drop concentration was sampled from the PDI, mounted on a wing pylon of the NASA P-3. The PDI uses interferometry with a diagnostic technique for sampling cloud droplet size and velocity at the same time (e.g., Chuang et al., 2008, Small et al., 2009). The combined range of 2 lasers with differing wavelengths covers liquid cloud droplets sized 1 to 1000 µm or larger.

CO concentration from the in situ sampled air is reported using the COMA instrument, which is the ABB/Los Gatos Research CO/CO2/H2O Analyzer modified for flight operations. It uses off-Axis ICOS technology to make stable cavity enhanced absorption measurements of CO, CO2, and H2O in the infrared spectral region, technology that previously flew on other airborne research platforms with a precision of 0.5 ppbv over 10 seconds (Provencal, et al., 2005; Liu, et al., 2017).

2.4 Local AERONET stations

New AERONET stations were set up for giving context to ORACLES measurements in south-western Africa along with the pre-existing stations in Henties Bay and Gobabeb, neighboring the SEA. In addition to the new permanent sites, the highly spatially resolved DRAGON (Distributed Regional Aerosol Gridded Observation Networks (Holben et al., 2018)) network of 6 AERONET stations were located near Henties Bay, about 100 km north of the NASA P-3 base station of Walvis Bay, Namibia, for the duration of ORACLES 2016. In addition to these stations, we use the data from the stations located at Walvis Bay Airport, Gobabeb, and Henties Bay in Namibia, and Lubango and Namibe in Angola. The reported data from these AERONET sites and DRAGON represent the entire span of available sampled full column AOD during the deployment time range, including potential local sources. To focus on the smaller aerosol of the lofted biomass burning aerosol (e.g., Pósfai et al., 2003) and reduce the influence of local sources such as large dust and sea salt aerosol particles, we report the fine mode AOD, derived using the Spectral Deconvolution Algorithm (O'Neill et al., 2003).

2.5 Satellites and climatology

Recent advances in satellite imager retrieval methodology enables the use of MODIS spectral cloud reflectances to obtain the overlying aerosol optical properties jointly with the cloud optical properties (Jethva et al., 2014; Meyer et al. 2015; Sayer et al., 2016). The algorithm used here, MOD06ACAERO (Meyer et al., 2015), simultaneously retrieves above-cloud AOD and the cloud optical thickness and effective radius of the underlying marine boundary layer clouds while also

© Author(s) 2019. CC BY 4.0 License.

providing pixel-level estimates of retrieval uncertainty that accounts for known and quantifiable error sources (e.g., radiometry, atmospheric profiles, and cloud and aerosol radiative models). MOD06ACAERO utilizes reflectance observations at six MODIS spectral channels from the visible to the shortwave infrared. Retrievals are run on both Terra (morning) and Aqua (afternoon) MODIS instruments under two aerosol model assumptions. The cloud forward model, ancillary data, and other retrieval assumptions are consistent with those of the operational MODIS cloud products (MOD06) (Platnick et al., 2017).

MODIS has been sampling aerosol since 2001 (Levy et al. 2013). Here we used the full time series of the fine mode AOD sampled in clear sky pixels in the SEA as a proxy for an ACAOD climatology similarly to Zuidema et al. (2016).

2.6 AOD above cloud determination

During ORACLES, we sampled multiple types of scenes, some of which were similarly described by Hobbs (2003), which had CAS (i.e., described in this paper as gaps) within aerosol layers and between aerosol and cloud layers. The AOD measurements that quantifies the aerosol above cloud in the presence of a gap, can extend thousands of meters vertically, because the aerosol within a gap contributes minimally to the overall ACAOD. For conditions without gaps, where the aerosol layer(s) are directly at the top of the cloud, the above cloud AOD is uniquely measured directly above cloud. To identify the measurements where 4STAR sampled ACAOD (including AOD measurements within a gap), we start with the periods of flights defined by the P-3 module flags as legs directly above cloud. These P-3 module flags were created using manual inspection of flight altitude time series and flight scientist mission notes from every flight (Diamond et al., 2018). We supplement these module flags with a manual inspection of the AOD time series from 4STAR, and select each sample measured directly above a cloud layer and up to the bottom of the aerosol layer. The cloud layer was defined by a cloud drop concentration greater than 10 cm^{-3} as measured by the PDI. When the PDI was not operational, we used lack of sun tracking from 4STAR, high relative humidity, and/or visual inspection of in-flight video as the metric for being in clouds. The bottom edge of the aerosol layer is defined at the altitude that has a 10% change in AOD and a dry scattering coefficient at 550 nm of either 50 Mm^{-1} or changed by more than 75% (Sect. 2.3). Figure 2 shows profiles with color-coded vertical regions to demonstrate the selection of the ACAOD portion of the AOD measurements.

3 Results and discussion

3.1 Statistics of sampled ACAOD and spatial distribution

We have separated all 4STAR measurements in the SEA into either ACAOD (11.5 hours of measurements) or full column AOD (0.9 hours of measurements), defined as measurements below 600 m in altitude. This subset of full column AOD is distinct from the ACAOD measurements as they necessarily require conditions without overlying cloud thus including the biomass burning layer of aerosol above clouds as well as any lower-level aerosol near the sea surface. We note that these two populations do not necessarily coincide directly, but may be

© Author(s) 2019. CC BY 4.0 License.

combined in a statistical sense. Figure 3 shows the distribution of those measurements at two wavelengths. The ACAOD at 501 nm ($ACAOD_{501}$) from all samples (blue bars) has a mean, median, and standard deviation of 0.32, 0.33, and 0.15 respectively. The full column AOD (pink bars) has a mean, median, and standard deviation of 0.36, 0.30, and 0.18, respectively. The larger mean AOD are likely representative of the combined aerosol burden from within the boundary layer as well as the typical plume observed aloft, although exhibiting larger variability as shown by the larger standard deviation. The small difference between the mean above cloud and full column AODs indicates that the majority of the AOD_{501} sampled in the region is due to the elevated layers of aerosol. In contrast, the AOD sampled at 1020 nm (AOD_{1020}) is much larger for the full column then its above cloud counterpart by nearly 70%, with the full-column AOD_{1020} having a mean, median, and standard deviation of 0.15, 0.13, and 0.06 respectively, and the $ACAOD_{1020}$ at 0.09, 0.09, and 0.05 respectively (Fig. 3b).
Considered together, the ACAOD and full column AOD (denoted by the total extent of the histogram bars in Fig. 3) represent what a satellite remote sensor would retrieve in the region, if it were spatially and temporally co-located to the NASA P-3 aircraft. The mean, median, and standard deviation of AOD_{501} for all combined measurements is 0.32, 0.33, and 0.15, respectively, though we note that this is dominated by the greater sampling of ACAOD vs full column AOD. The average, median, and standard deviation of uncertainty in ACAOD sampled by 4STAR due to instrumental artifacts and calibration (see appendix for more details) is 0.011, 0.01, and 0.008 (0.013, 0.012, and 0.012) at 501 nm (1020 nm).

The spatial distribution of the $ACAOD_{501}$ is presented in Fig. 4. The ACAOD was averaged in nearly equidistant latitude and longitude bins (0.65° latitude by 0.6° longitude). We observe highest ACAOD near the western coast of Africa at the northernmost parts of the sampled region, while the lowest ACAOD is in the south of the sampled region. The higher ACAOD is observed to extend to the west but at reduced AOD compared to near coast, consistent with the expected behavior of the climatological plume (Fig. 1 and Zuidema et al., 2016). The higher average ACAOD in the northernmost part of the sampled region is also observed in the fine mode AOD from ground based AERONET stations along the southern African coast (triangle symbols in Fig. 4).

The variability in standard deviation shows that in the north variability is low in measured ACAOD (Fig. 4b). Note that the standard deviation here is calculated as a fraction of all samples, though we show the total number of flight days contributing to each bin to give context as to the temporal variability observed. The largest variability of the sampled ACAOD seems to be concentrated in the central portion of the measured region, around 18°S and 8°E, with ACAOD standard deviation exceeding 0.15, over the 3 - 5 days sampled. This high variability is consistent with a day-to-day change in the location of the southern edge of the highest AOD in the aerosol plume climatology for September (Fig. 1 and Zuidema et al. 2016). Large variability is also observed near Walvis Bay, Namibia, outside the typical climatology for the biomass burning plume. This variability in ACAOD is likely caused by local production of aerosol, observed to be mostly dust or large particles. This hypothesis is corroborated with ground-based measurements from an AERONET station located at the Walvis Bay Airport which shows a large but variable coarse mode fraction of AOD, and consistently larger aerosol effective

© Author(s) 2019. CC BY 4.0 License.

radius from sky scan retrievals. The fine mode fraction of the AOD sampled by AERONET near the Walvis Bay Airport also shows some variability (Fig. 4b), but this is dwarfed by the coarse mode variability (not shown).

An average ACAOD of this region can be calculated from these binned spatial statistics, representing a more even weighting of the ACAOD (equal spatial bins) as compared to averaging over the total number of samples which could be influenced by variability in sampling density. The mean $ACAOD_{501}$ and its uncertainty is 0.37±0.01, which is arguably more representative of the SEA region, as determined by the average of the mean within each spatial bin. The median $ACAOD_{501}$ of the region is 0.34±0.01 and the average standard deviation is 0.05±0.004. The above averaging method attempts to reduce the spatial sampling bias from sampling the same area multiple times (like for the relatively low ACAOD near Walvis Bay), but at a cost of temporal resolution. The equivalent spatially averaged, median, and average standard deviation of $ACAOD_{1020}$ is 0.11±0.02, 0.09±0.01, and 0.02±0.004.

3.2 Spectral AOD above cloud and its Ångström Exponent (AE)

The spectral characteristics of AOD above cloud is related to the aerosol intensive properties (shape, size distribution, absorption, and refractive index) (e.g., Kaskaoutis and Kambezidis, 2008, O'Neill et al., 2001). From all measurements of ACAOD at wavelengths outside strong gas absorption, we created ACAOD spectra representing the mean, median, and related standard deviation (Fig. 5), which is representative of the sampled ACAOD throughout this deployment, having the same mean, median, and standard deviation of the ACAOD at 501 nm and 1020 nm presented in Fig. 3. The ACAOD spectra for both the mean (0.38 at 452 nm; 0.13 at 865 nm) and median (0.38 at 452 nm; 0.12 at 865 nm) are easily within the mean uncertainty (0.013 at 452 nm; 0.008 at 865 nm) of the measured spectra. The standard deviation of the ACAOD (0.18 at 452 nm; 0.06 at 865 nm) is nearly equivalent to its mean at the longest wavelengths (longer than 1600 nm). This larger standard deviation at longer wavelengths can be caused by sporadic larger AODs at those longer wavelengths, agreeing with the notion of intermittent presence of dust or marine aerosol, or alternatively, this may be linked to lower signal to noise ratio of the 4STAR spectrometers.

The relationship of the AOD at various wavelengths is used to determine the Ångström exponent (AE, or sometimes referred to the extinction Ångström exponent) (Ångström, 1929), which is inversely related to the size of the aerosol particles. The AE for the sampled AOD is not only dependent on the size distribution of aerosol particles but also on the type of aerosol measured (e.g., Russell et al., 2014). As a first approximation, large aerosol particles will typically record small AE values and vice-versa (e.g. an AE value between 0.1 and 1 for large marine aerosols (Sayer et al., 2012) or above 1.5 for small biomass burning or urban industrial aerosols (Russell et al., 2014, Fig 6, LeBlanc et al., 2012)). According to Dubovik et al., (2002), AERONET-derived AE values (computed between 440 and 870nm) for biomass burning aerosols are between 1.2 and 2.1 in Bolivia or Brazil, whereas AE values from desert dust aerosol are between 0.1 and 0.9 in Saudi Arabia. The AE measured in the source regions of the biomass burning from SAFARI-2000 showed a range between 1.6 and 2.1 from Mongu, Zambia

© Author(s) 2019. CC BY 4.0 License.

during the biomass burning season (Eck et al., 2003). Here we evaluate AE using two methods: 1) by fitting a second-order polynomial to the logarithm of the AOD spectra from selected wavelengths between 355 nm to 1650 nm and finding its derivative at any one wavelength, (here at 500 nm, AE_{500}) (e.g., O'Neill et al., 2001; Shinozuka et al., 2011) (Figure 6a), and 2) the negative of slope of the AOD with wavelength in logarithmic scale (two wavelengths used here 470 nm and 865 nm, $AE_{470/865}$) (e.g. Dubovik et al., 2002) (Figure 6b).

In Fig. 5, the mean and median AOD spectra are not a straight line in the log-log plot but rather curves slightly, indicating that the AE is not wavelength independent. The curvature of AE (spectral dependence of the AE), like its value, is related to the aerosol size distribution (e.g., Kaufman, 1993, Eck et al., 1999, O'Neill et al., 2001, Yoon et al., 2012) and additionally to the aerosol absorption (Kaskaoutis and Kambezidis, 2008). The two methods to calculate AE (evaluated at different wavelengths) can also be used to help illustrate the AE curvature:

There is a distinction between mean AE from ACAOD vs. full column AOD observed for both methods, AE_{500} and $AE_{470/865}$. The mean AE_{500} for ACAOD and full column are 1.45 and 1.08, while the mean $AE_{470/865}$ are 1.71 and 1.25, respectively (see blue and pink solid lines in Fig. 6). The distribution of AE in Fig. 6 seems to indicate that most of the ACAOD is influenced by fine-mode aerosol particles, which is consistent with aerosol that are aged biomass burning as reported by Eck et al. (1999) and with the aerosol in situ sizing measurements taken on board the NASA P3. The difference in average AE evaluated at different wavelengths, (AE_{500} - $AE_{470/865}$) is -0.26 for the ACAOD, which is very similar to the AE difference (centered at about -0.2 for similar metrics) sampled by the Mongu AERONET station within the biomass burning source region of southern Africa (Yoon et al., 2012). The full column average AE difference of 0.17 is typical of coarse-mode dominant marine aerosols (Yoon et al., 2012) corroborated by the in situ measurements of large marine aerosol particles during the boundary layer flight segments during ORACLES.

From the AE information alone, we have a sense of the particle size but without more advanced aerosol classification methods, such as the pre-specified clustering method in Russell et al. (2014), which utilize additional aerosol intensive properties (such as the Single Scattering Albedo at different wavelengths or the Refractive Index), we refrain from inferring aerosol composition.

The spatial patterns (Fig. 7) of the above cloud AE help indicate the potential changes in aerosol intensive properties measured during ORACLES 2016. For the sampled region, the spatial mean $AE_{470/865}$ (AE_{500}), obtained by averaging the mean of each bin over the entire region, is 1.65 (1.44), with a spatial average of the medians is 1.66 (1.48), and a spatial average of the standard deviation within each bin of 0.10 (0.06). This spatial averaging method is similarly used in Section 3.1. The spatial statistics of $AE_{470/865}$ and A E_{500} for the full column AOD is lower than its ACAOD counterpart by 0.4 for the mean and by 0.3 for the median, with similar standard deviations. The smallest $AE_{470/865}$ is observed in locations near coast in the northern part of the sampling region, albeit with few sampling days within each bin, and south of the routine flight paths. A distinctively smaller than average $AE_{470/865}$ value is also observed near

© Author(s) 2019. CC BY 4.0 License.

Walvis Bay, Namibia. This low $AE_{470/865}$ may be coincident with dust or marine aerosol within the sampled column of ACAOD sampling at altitudes of 300 to 3700 m. Further from the coast, there is a small tendency towards decreasing AE values, present in multiple flights, from about 1.8 to 1.6 at 5°E to 3°E. At those same locations (not shown), the AE_{500} does not show a similar trend, possibly indicating a change in aerosol composition and size. There is however a trend of higher AE_{500} near the center of the region (7°E to 11°E and 20°S to 15°S), by more than 0.2 as compared to the furthest west points. Similar to the map of the standard deviation of the ACAOD (Fig. 4), a larger standard deviation in AE is observed near 18°S and 8°E, at the variable southern edge of the climatological mean aerosol plume, in the area with multiple sampling days. Further northwest, a nearly equivalent number of days were sampled, but the standard deviation of the $AE_{470/865}$ is lower, indicating lower natural variability. In the northern near coast region, there are multiple bins that were sampled during only one day; here the standard deviation should not be taken to represent the actual variability of the aerosol, but rather of the sampling accuracy within a day.

3.3 Airborne AOD in context of climatology and satellite measurements

To contextualize the ACAOD sampled during the ORACLES 2016 measurements, we compared the ACAOD measured directly below the aerosol layers from the NASA P-3 to those retrieved from MODIS satellite measurements. We focus on the diagonal routine flight paths (South-East to North-West), where the P-3 sampled the same locations numerous times over the course of the month-long deployment. The sampled ACAOD for each of the routine flights (identified by their day in Fig. 8a) is compared to its equivalent retrieved from the combination of MODIS sensors from Aqua and Terra using the MOD06ACAERO methodology described by Meyer et al. (2015) (Sect. 2.5). When comparing ACAOD from 4STAR and MOD06ACAERO for each sampling day, a general agreement for most days is observed with some high deviations at certain longitudes for MOD06ACAERO, albeit with high day-to-day variability. Higher than average ACAOD was measured by both 4STAR and MOD06ACAERO near 3°E on 31 August and 4 September, while MOD06ACAERO was high compared to 4STAR measurements on 12 September near 7°E.

We compile daily 4STAR ACAOD and MOD06ACAERO values to a mean and median, which is compared to a proxy ACAOD climatology (Fig. 8b & 8c). The MODIS fine mode clear sky AOD from 12 years during the months of September and August (Wood et al., In prep) represent the proxy for the ACAOD, which is fine-mode dominant aerosol as observed with the high AE measurements and in situ observations. The general longitudinal dependence and magnitudes of the mean ACAOD as measured by 4STAR are consistent with the MODIS fine mode climatology, with larger ACAOD in the western region (Fig. 8b).

The peak in the climatology occurs near 1°E, whereas the sampled peak from 4STAR ACAOD is closer to 3°E, and MOD06ACAERO subsampled to routine flights is closer to 2°E. The larger mean MOD06ACAERO at 7°E as compared with 4STAR and climatology is likely due to anomalously high days skewing the mean (such as 12 September). On the eastern end, 4STAR measured much lower ACAOD (below 0.1) than the climatology and MOD06ACAERO between 10° - 12°E, but higher (>0.25) at the easternmost edge of the routine flight path, near 14°E.

© Author(s) 2019. CC BY 4.0 License.

4STAR easternmost measurements are within 0.05 of the averages from AERONET ground based measurements over the same routine flight days, which is higher by ~0.15 than monthly averages from AERONET measured during August or September 2016. For the entire longitude span investigated here, 4STAR ACAOD averaged 12.2% lower than the climatology (difference of 0.04 AOD), and 16.0% lower than MOD06ACAERO for September (12.1% of the August mean) along the routine flight track.

The longitudes with the smallest difference between the subsampled MOD06ACAERO and the monthly averages indicates that the routine flight sampling for those regions reflect the monthly mean, whereas for regions with large differences, the sampling is not representative of the mean monthly values. The peak August and September mean ACAOD from MOD06ACAERO at the most western edge of the region, near 0°E, is shifted to the east in the subsampled MOD06ACAERO.

The largest differences between the monthly mean MOD06ACAERO for September 2016 and the subsampled MOD06ACAERO (around 2°E, 6°-7°E, and 10°E), suggest that sampling in that region is not representative of the monthly mean, whereas there is good agreement between the subsampled and the monthly mean in other longitudes suggesting that the flights which followed the routine path can be used to infer monthly statistics. By extension, the sampling from 4STAR ACAOD measurements are representative of the monthly mean ACAOD for the same longitudes that the subsampled MOD06ACAERO matches the September 2016 mean, albeit with a bias of about 0.05 - 0.08 for most of the flight tracks (4STAR being lower than the subsampled and monthly mean MOD06ACAERO). There is a divergence near coast (12°E) between 4STAR ACAOD and MOD06ACAERO, showing a longitudinal trend in this bias by greater than 0.1.

Similar longitudinal dependence of ACAOD is observed in the medians as with the means, but with greater differences at most longitudes between 4STAR ACAOD and MOD04ACAERO. Differences between the mean and the medians are shown here to reduce impact of outliers in our sparsely sampled data. The MODIS fine mode climatology medians peaks twice in the western edge, near 1°E and 4°E, whereas the measured 4STAR ACAOD peaks at 1°E, and MOD06ACAERO also peaks at 1°E, and again at 7°E, like its means. Median and mean differences for both MOD06ACAERO and 4STAR seem to move their respective maximum further west, and increase matching further east (notably at 9°E), indicating a changing ACAOD distribution with longitude.

Overall, the sampled ACAOD by 4STAR is slightly lower than the MOD06ACAERO counterpart for averages and medians over the same days, additionally, it is lower than the MODIS AOD fine mode climatology. The peak for September 2016 was more eastward than what the MODIS AOD fine mode climatology would indicate, more so as measured by 4STAR than MOD06ACAERO. This shift in peak ACAOD is likely related to differences in wind patterns or shifting of the biomass burning locations for September 2016 as compared to the 12 year climatology.

© Author(s) 2019. CC BY 4.0 License.

3.4 Vertical profiles of aerosol optical properties

3.4.1 Spatial variability in AOD profiles

The vertical distribution of the measured ACAOD is presented in Fig. 9. Here, we show a subset of the AOD_{501} profiles divided into northern vs southern geographic regions to compare coastal flights (Fig. 9b & 9d) versus along the further-from-coast routine diagonal (Fig. 9a & 9c). Of particular interest are the considerably high values (>0.5) of AOD_{501} observed in coastal flights at the base of the aerosol plume, compared with similar altitudes (about 2500 m) along the routine diagonal region. The top of the aerosol plume for all these profiles are within the range of 4000 m to 6000 m. In these altitude profiles, which show column AOD of the aerosol only above the aircraft at a given time, a near vertical AOD trace (i.e. no change of AOD with height) denotes a vertical range where the aerosol content is low or its contribution to the total optical depth is marginal, i.e., a gap. Although variability is observed, particularly farther from the coast, such near-vertical lines occur more often and for larger vertical distance along the routine diagonal. Similarly, a negative slope with altitude denotes the presence of aerosol with large impact on the total optical depth. As expected, for the observed profiles, this feature coincides with high concentration of the in situ biomass burning tracer CO (above 200 ppbv) measured from the COMA instrument.

Although generalities can be inferred from these profiles, a high degree of variability is noticeable, especially when contrasting the far-from-coast versus profiles along the routine diagonal. This variability is more commonly found in the presence of a gap between cloud and aerosol and its vertical distance. For the coastal flights, the vertical distance ranges from 0 - 2500 m, while the routine flights it is 0 - 4000 m. As an indicator of the variability of the AOD profile in these different regions, we observed at 2000 m AOD ranges between 0.17 to 0.6 for profiles along the routine diagonal, and 0.3 to 0.58 for coastal profiles. The vertical thickness of the plume itself is also generally larger in the northern regions (Fig. 9a & 9b), consistent with the climatological understanding of the plume spatial and vertical location (Zuidema et al., 2016).

3.4.2 AE vertical dependence

Considering all measurements made during ORACLES 2016 from the P-3, the $AE_{470/865}$ is roughly constant at a median value of 1.75 between an altitude of 600 m and 6 km, whereas below that, the median decreases monotonically to 0.6 (Figure 10), observed in all data and the ACAOD subset. The ACAOD $AE_{470/865}$ above 3000 m increases up to 2.1, diverging from $AE_{470/865}$ from all data. Although this may indicate a trend, the low sampling (less than 3 days, denoted by the light color shading) for the ACAOD data at those altitudes may simply be spurious as compared to $AE_{470/865}$ at the same altitude calculated from all AOD, regardless if they do not represent the full column of aerosol above clouds. The relatively consistent $AE_{470/865}$ with altitude is an indicator of a constant aerosol particle size distribution throughout the vertical layer, above 600 m. Below that, the much smaller average $AE_{470/865}$ is a telltale sign of larger aerosol particles near sea surface, and is reproduced over more than 9 days sampled. The mean and median are vertically uniform, but there is a larger variability at higher altitudes, especially near 4800 m compared with lower altitudes.

© Author(s) 2019. CC BY 4.0 License.

3.4.3 Hyperspectral ACAOD profile example

For a singular case, 4STAR's hyperspectral sampling allows analysis of AOD at multiple wavelengths, covering a vast spatial region including vertical flight profiles thereof. Figure 11 shows hyperspectral AODs retrieved through the aerosol layer above for a selected flight segment on 20 September 2016. This case, sampled near 16.7°S and 8.9°E, has a full-column ACAOD of 0.63 at 501 nm. No gap is observed between cloud top (950m; bottom of profile) and the aerosol layer. There are, however, changes in AOD gradient with altitude, indicating variable aerosol extinction with altitude, likely due to vertical structure of aerosol concentration or type within the full aerosol plume. The top of highest aerosol layer extends to about 5916 m, with minimal change in AOD is observed above that altitude.

AOD measured here has a smoothly varying dependence on wavelength in the ultraviolet to near-infrared wavelength range. This vertical profile of AOD shows a mostly constant wavelength dependence of the AOD at differing altitudes (Fig. 11b). In addition to the AOD, we included total optical depth of the column, which has the contributions of strongly absorbing gas components (water vapor, oxygen-a band) in shaded wavelength regions. The vertical profile (Fig. 11a) is not always continuous, with some breaks in AOD measurements linked to sampling issues, such as a momentary loss of sun-tracking through a spiral maneuver of the aircraft found at 3500 m of altitude. The AOD spectra at different altitude (Fig.11b) is seen to be mostly smoothly varying, except for locations of low signal to noise of the 4STAR's detectors, such as the longest wavelength region near 1600 nm, and at wavelength regions near 430 nm, where a slight 'bump' over the smoothly varying spectra are observed and likely linked to signal issues of the detectors.

Figure 12 shows this case at specific wavelengths for AOD (Fig. 12a), as well as the $AE_{470/865}$ as an indicator of above aircraft aerosol particle size (Fig. 12b). The $AE_{470/865}$ does not change significantly from 1.75 for altitudes up to 4500 m, above which it is reduced down to 1.25 corresponding with low AOD (<0.05). The aerosol extinction coefficient can also be derived for the AOD vertical profile (Fig. 12c) by using the differential of AOD with respect to altitude change with a smoothing of 50 seconds (similarly to Shinozuka et al., 2013). This extinction coefficient compares well to the in situ extinction coefficient (Fig 12d), derived using the HiGEAR's nephelometers for scattering coefficient adjusted to ambient relative humidity and the dry absorption coefficient measured using the PSAP. Slight deviation between the extinction coefficient calculated from 4STAR AOD and in situ measurements are likely linked to differing relative humidity dependence of the aerosol particles, and its adjustments. We see that regions of high extinction coefficient coincide with elevated CO concentration for this profile (Fig. 12e).

3.5 AOD distance to cloud

The vertical profiles of AOD presented in Fig. 9 showcase the large variability in the gap size and location along the atmospheric column. Namely, some profiles show a gap between the aerosol layer and the clouds, some show no gap, and some show a gap between two aerosol layers. Examples of these cases have been collected via photography from the NASA P-3 and are shown in Fig. 13, similarly portrayed by Hobbs (2003). These photographs were selected for easier visual identification, although not always showing scenes with 100% cloud cover. Aerosol

© Author(s) 2019. CC BY 4.0 License.

appears visually darker than the background light blue sky when the observer is at or below the altitude of the aerosol layer (Fig. 13a & 13b). When the aerosol appears directly above clouds, it can be interpreted as a lighter colored haze extending from cloud top, sometimes making it harder to distinguish between aerosol and cloud boundaries (Fig. 13c).

The ACAOD flag, described in Section 3.2.3, allows assessment of the frequency of cases where there is and is not a gap between aerosol layer and cloud, (Fig. 13b & 13c), though is not able to identify more complex scenes with a gap within aerosol layers. During any one profile, the vertical extent of the measurement flagged to be an ACAOD represents the gap between cloud top and aerosol layer bottom. For cases where this vertical extent is near 0 m (within an uncertainty of 60 m), it is said that this profile has no gap between aerosol and cloud. Unlike both previous studies from spaceborne lidars (Sakaeda et al., 2011; Rajapakshe et al., 2017), we found the longitudinal dependence of this gap does not uniquely follow a linear decreasing relationship with westward movement (Fig. 14). Expectations of the gap extent from CALIOP (Wood et al., In prep) were matched for far-from-coast profiles with the smallest gap extent observed at longitudes westward of 2.0°E, albeit with a low number of days sampled (only a maximum of 3 days, with 6 different profiles). The largest average gap is not nearest to coast as expected, but rather midway in this sampling region at about 7.5°E, and is observed over 5 distinct days. Similarly, a local maximum in gap extent near 7.5°E is described by Rajapakshe et al. (2017) using observed in nighttime CATS and CALIOP measurements. Nearer to coast between 8.5°E and 11.5°E, there is a region of smaller to near zero gap extent, with median extents below 500 m. Combined together in larger longitude spans (Fig. 14b, 14c, and 14d), omitting the profiles taken over land during take-off and landing at 14.5°E, the mean of the gap extent distribution peaks between 5°-10°E, not as expected from the CALIOP analysis. Another way to view this distribution's dependence with longitude is the proportion of the total profiles or cases that have a gap of less than 60 m (near zero for this analysis), or through the larger distance defined as Clouds embedded within an Aerosol Layer (CEAL; 360 m) by McGill et al. (2015), denoted by the dark and light gold colors in Fig. 14. We see a region where 0% of the 4 profiles measured a near zero gap extent at 5.5°E and 0% of the 16 profiles are considered CEAL cases at 5.5°E to 7.5°E . The peak of the cases that have no gap or CEAL occur at the westernmost edge, with a secondary peak between 8.5°E to 11.5°E. For all measured profiles, the proportion of CEAL cases is observed here at 48%, a statistically significant lower value (p-value of 0.027) than reported for a larger region sampled with CATS (60%) by Rajapakshe et al. (2017).

4 Summary and Discussion

During the ORACLES 2016 campaign, the NASA P-3 sampled aerosol above the marine stratocumulus clouds in the South-East Atlantic during the month of September, coinciding with the peak of the biomass burning season in Sub-Saharan Africa. The 4STAR instrument, on board the P-3, sampled the AOD from a range of flight altitudes, a portion of which is defined as ACAOD. The ACAOD is presented here in terms of distribution of its magnitude, spatial dependence, vertical variability, and spectral dependence.

© Author(s) 2019. CC BY 4.0 License.

For all measured spectral AOD during September 2016, we show in Table 1 different statistics (mean, median, and standard deviation), calculated from all measurements equally, and the another utilizing spatial binning followed by averaging. By calculating the mean, median, and standard deviation from all measurements, we inherently give more weight to the areas most often sampled during the field campaign, such as the routine flight paths, whereas the spatial binning of these statistics represents a more evenly weighted representations of the measured values. Here we see that the mean spatially binned ACAOD is higher than from all measurements, indicating that we disproportionally sampled low ACAOD regions, similarly for the Total AOD, and ACAOD uncertainty. The spatially binned AE is smaller than its all measurement counterpart, showing that our sampling strategy favored smaller aerosol particles.

Observed variations from the mean during the sampling period have been showed to be significant, from changes in spatial patterns to changes in vertical profiles. The spatial pattern of the ACAOD shows that the largest optical depth is found in the northern region near coast, where 12 years of MODIS AOD sampling shows the most optically thick aerosol plume. Along the diagonal flight path, measured during routine flights from the NASA P-3, the lowest ACAOD is observed at the southern end, with the largest variability of ACAOD midway, linked to the aerosol plume's southern edge latitudinal movement. This region of high ACAOD variability coincides with high variability of the $AE_{470/865}$ derived from the ACAOD spectral dependence. Together this indicates that we sampled a majority of small aerosol particles, linked to biomass burning, as expected, albeit with larger variability in aerosol size or composition near the southern edge of the climatological plume. For the full column AOD, the $AE_{470/865}$ is much lower than its above cloud counterpart, linked to large aerosol particles, such as marine aerosol embedded within the boundary layer.

When comparing to satellite measurements and long term AOD measurements in the region, the measured ACAOD is lower than both coincident MOD06ACAERO retrievals and the long-term fine mode MODIS AOD average over the region. 4STAR systematically returning lower ACAOD by 0.05 - 0.08 than MOD06ACAERO. The ACAOD from 4STAR also has a peak closer to shore than the MODIS AOD climatology mean and median (both fine and coarse mode), with differences near coast between 4STAR ACAOD measurements and MOD06ACAERO retrievals.

Differences in vertical AOD profiles are indicative of the variability of the altitude and magnitude of the aerosol plume. We have observed distinct AOD profiles along the routine diagonal and for coastal flights. Coastal flights had typically larger AOD at high altitude (averaging larger than 0.5 at 2500 m altitude) as compared to flight along the routine diagonal (lower than 0.5 at 2500 m altitude). The vertical extent where the AOD does not change significantly, linked to a gap between aerosol and cloud, spans a larger distance further from coast than near coast (0-4000 m far-from-coast, 0-2500 m near-coast). Where there is a strong decrease in AOD with increasing altitude coincides with locations of high concentrations of CO, a tracer of biomass burning. The derived extinction coefficient from 4STAR AOD profiles and in situ measurements appear to match very well for one example shown. In the vertical domain, the AOD is observed to be spectrally smooth with a nearly constant $AE_{470/865}$ vertically for the majority of the

© Author(s) 2019. CC BY 4.0 License.

measurements, only significantly reducing near surface. The gap vertical extent calculated from 4STAR data, in conjunction with in situ measurements of scattering coefficient and cloud drop concentration, appears to have a more complex dependence with longitude than initially expected from CALIOP space-borne observations. Visual observations from the NASA P-3 flights corroborate previous observations of clear air slots, and their inherent variability. There is a prevalence of near zero gap extent, while the largest gaps extents are observed not as expected but off-shore near 7° W. We have also observed a lower proportion of cases where the aerosol layer is near the cloud top as compared to previous studies (48% of CEAL instead of the 60% reported using CATS by Rajapakshe et al. (2017)

From these airborne measurements, we have seen that the ACAOD is lower than expected from current MODIS satellite retrievals during the measurement period (by 0.05-0.08) and from a 12-year climatology (by 0.04). We have also observed the largest variability in aerosol optical properties (ACAOD and AE), at the southern edge of the climatological aerosol plume for September. The vertical dependence of the ACAOD was very variable, even for the same regions, with aerosol layer tops ranging from 4000 m to 6000 m, while their bottoms were from 400 m to 4000 m. We observed the extent of the gap between aerosol and cloud to peak at a longitude of 7.5°E, unlike the expectation of a gradual decrease of this gap as the aerosol plume moves westward, further from coast.

A Appendix: Description of 4STAR data quality

AOD sampled by 4STAR is subject to various sources of measurement uncertainty, with changes of calibration during the field mission linked to changing spectrometer throughput, and during flight linked with window contamination and angular response to radiometric calibration of the 4STAR head. These corrections and processing are combined within the 4STAR's open source processing code (4STAR Team, 2018)

A.1 4STAR calibration and performance

To quantify the atmospheric transmission of light used to calculate AODs from 4STAR, we calculate the incident light as seen by 4STAR at the top of the atmosphere, its calibration coefficients, by using a refined Langley extrapolation method based on the Beer-Lambert law (Schmid and Wehrli, 1995). To create this Langley extrapolation, we use measurements near sunrise and sunset (a spread of airmass factor from 1.8 to 12) taken weeks before and after the observation campaign at the high-altitude Mauna Loa Observatory (MLO) in Hawaii, under minimally-polluted conditions. Using similar metrics to those described by Shinozuka et al. (2013), the relative standard deviation of the calibration derived from 6 Langley extrapolations during pre-deployment MLO is 0.63% (0.17%) at 501 nm (1040 nm). For post-deployment MLO, this relative standard deviation calculated from 4 Langley extrapolations is 1.2% (0.39%) at 501 nm (1040 nm). The calibration from the post-deployment MLO Langley extrapolations shows a decrease of 2.9% (an equivalent maximum AOD of 0.029 when sun is overhead) at 501 nm and an increase of 0.2% (equivalent to 0.002 AOD) at 1040 nm as compared to pre-deployment MLO. This variation between the pre- and post-deployment MLO calibration can be attributed to a disconnection of the fiber optic linking the 4STAR head and the spectrometers during the time

© Author(s) 2019. CC BY 4.0 License.

between the MLO pre-deployment calibration and the ORACLES deployment. Subsequent disconnections did not occur.

For added traceability of the calibration during the ORACLES deployment, we incorporate AOD measured from high altitude, low aerosol loading conditions when 4STAR was effectively sampling the stratospheric AOD contribution. During ORACLES, the AOD derived from 4STAR measurements were sensitive to relative humidity variations of the spectrometers, when failure of the humidity control occurred (desiccant was depleted). To account for this variation, a set of new calibrations was obtained from the average of Langley extrapolation obtained during post-deployment MLO, Langley extrapolation during high altitude flight segments with airmass factor changes of greater than 2 (similar to method described by Shinozuka et al. (2013)), and from calibrations derived from matching a reference stratospheric AOD spectrum to high altitude high sun measurements. The reference stratospheric AOD spectrum is obtained from the lowest AOD measured at the AERONET (Holben et al., 1998) Bonanza, Namibia, site (an altitude of 1.3 km) over the course of 3 months, which was found to be 0.016 at 501 nm, and then a log-log second-order polynomial fit (e.g., Shinozuka et al., 2013) was used to interpolate the reference AOD spectrum to wavelengths sampled by 4STAR. From this method, a total of 7 set of calibrations were applied to 4STAR, separating periods of varying relative humidity of the enclosure with the spectrometers. The relative standard deviation of all these calibrations is 0.83% (1.12%) at 501 nm (1040 nm). Similar performance from 4STAR has been observed in previous field campaigns (e.g., Shinozuka et al., 2013), where extensive comparisons to ground based AERONET stations resulted in a root-mean-square difference of 0.01 for wavelengths between 501 nm and 1020 nm, 0.02 at 380 and 1640 nm, and 0.03 at 440 nm.

A.2 4STAR corrections and uncertainty

Accurate 4STAR measurements of AOD require corrections for some instrument artifacts and impact of light absorption by trace gases. Corrections related to light transmission variations due to angular variability of the fiber optic rotating joint (FORJ), due to deposition of material on the outside window of 4STAR's sun barrel, and finally atmospheric trace gases contribution to AOD estimates.

Correcting light transmission variability due to the FORJ uses azimuthal position of the 4STAR sun-tracking head in relation to the plane's axis. This azimuthal dependence is measured in between each flight by a full rotation in each direction while staring at a stable light source (a light emitting diode that has less than 0.1% variation in radiance during the time of the test is used here). The variations have a near sinusoidal shape with features departing from the mean by no more than 1.4% and are repeatable in between each measurement (within 0.2% over the course of the field mission), with the largest features not moving by more than 30 degrees.

The impact of window deposition on the transmission of 4STAR's sun barrel is quantified by measuring the change in signal from a stable light source before versus after cleaning the window, and is performed after each flight. We attributed any window deposition observed to discrete events during flight, notably during low-level near water flight segments or during cloud insertions. The uncertainty of the AOD surrounding these events (within +/- 20 minutes) have

© Author(s) 2019. CC BY 4.0 License.

been increased to the magnitude of the window deposition's optical depth, and by 30% of the corrected magnitude for the rest of the flight, producing a step-change in the AOD uncertainty. The impacts of these events were quantified by the change in high altitude AOD before and after the low-level segments. Differences of larger than 2% but not more than 4.5% occurred in 4 of the 15 research flights and have been corrected, both the magnitude of the AOD and its related uncertainty, using the above described method.

AOD is influenced by trace gas absorption in the entire column in distinct wavelength regions. We correct the influence of trace gas (NO_2, CO_2, O_3, O_2-O_2, CH_4) by convolving their retrieved vertical column gas abundance and profile with their spectral absorption coefficients (Segal Rozenhaimer et al., 2014). This result in an optical depth contribution from these gases (typically very minor) which is then subtracted from the AOD spectrum.

Data availability

All ORACLES-2016 in situ data used in this study are publicly available at https://doi.org/10.5067/Suborbital/ORACLES/P3/2016_V1 (ORACLES Science Team, 2017). This is a fixed-revision subset of the entire ORACLES mission dataset. It contains only the file revisions that were available on 15 June 2018.

Author Contributions

SL and JR conceived the study. JR acquisitioned the funding. SL and KP analyzed the data with help from CF, ML, MSR, YS, and SGH. YS helped in curating the data from ORACLES. SL, CF, KP, MK, MSR, YS, JP, SGH, SF, and JSG collected data on board the NASA P3, while AERONET data was collected by BH, PF, SP, GMK, MG, and AN. KM provided satellite data and analysis. SD and RPD provided engineering support for 4STAR. SL wrote the paper with reviews from all authors.

Acknowledgments

The authors wish to acknowledge all of the ORACLES science team and the NASA P-3 flight and maintenance crew for the successful deployment. ORACLES is funded by NASA Earth Venture Suborbital-2 grant NNH13ZDA001N-EVS2. The Henties Bay and Gobabeb AERONET stations are maintained by the French Centre National de la Recherche Scientifique (CNRS) and the South African National Research Foundation (NRF) through the "Groupement de Recherche Internationale Atmospheric Research in southern Africa and the Indian Ocean" (GDRI-ARSAIO), the "Projet International de Coopération Scientifique" (PICS) "Long-term observations of aerosol properties in Southern Africa" (contract n. 260888), and the Partenariats Hubert Curien (PHC) PROTEA of the French Ministry of Foreign Affairs and International Development (contract numbers 33913SF and 38255ZE).

© Author(s) 2019. CC BY 4.0 License.

References

4STAR Team, Samuel LeBlanc, Connor J Flynn, Yohei Shinozuka, Michal Segal-Rozenhaimer, Kristina Pistone, Meloë Kacenelenbogen, Jens Redemann, Beat Schmid, Phillip Russell, John Livingston and Qin Zhang: 4STAR_codes: 4STAR processing codes, doi:10.5281/zenodo.1492912, 2018.

Ångström, A.: On the Atmospheric Transmission of Sun Radiation and on Dust in the Air, Geogr. Ann., 11(2), 156–166, doi:10.1080/20014422.1929.11880498, 1929.

Bergstrom, R., Pilewskie, P., Schmid, B. and Russell, P. B.: Estimates of the spectral aerosol single scattering albedo and aerosol radiative effects during SAFARI 2000, J. Geophys. Res., 108(D13), 1–11, doi:10.1029/2002JD002435, 2003.

Bond, T. C., Doherty, S. J., Fahey, D. W., Forster, P. M., Berntsen, T., Deangelo, B. J., Flanner, M. G., Ghan, S., Kärcher, B., Koch, D., Kinne, S., Kondo, Y., Quinn, P. K., Sarofim, M. C., Schultz, M. G., Schulz, M., Venkataraman, C., Zhang, H., Zhang, S., Bellouin, N., Guttikunda, S. K., Hopke, P. K., Jacobson, M. Z., Kaiser, J. W., Klimont, Z., Lohmann, U., Schwarz, J. P., Shindell, D., Storelvmo, T., Warren, S. G. and Zender, C. S.: Bounding the role of black carbon in the climate system: A scientific assessment, J. Geophys. Res. Atmos., 118(11), 5380–5552, doi:10.1002/jgrd.50171, 2013.

Chand, D., R. Wood, T. L. Anderson, S. K. Satheesh, and R. J. Charlson: Satellite-derived direct radiative effect of aerosols dependent on cloud cover, Nat. Geosci., 2, 181-184, doi:10.1038/ngeo437, 2009.

Chang, I. and Sundar, C. A.: The impact of seasonalities on direct radiative effects and radiative heating rates of absorbing aerosols above clouds, Q. J. R. Meteorol. Soc., 143(704), 1395–1405, doi:10.1002/qj.3012, 2017.

Chuang, P. Y., E. W. Saw, J. D. Small, R. A. Shaw, C. M. Sipperley, G. A. Payne, and W. D. Bachalo: Airborne Phase Doppler Interferometry for Cloud Microphysical Measurements, Aerosol Science and Technology, 42:8, 685-703, DOI: 10.1080/02786820802232956, 2008

Diamond, M. S., A. Dobracki, S. Freitag, J. D. S. Griswold, A. Heikkila, S. G. Howell, M. E. Kacarab, J. R. Podolske, P. E. Saide, and R. Wood: Time-dependent entrainment of smoke presents an observational challenge for assessing aerosol–cloud interactions over the southeast Atlantic Ocean, Atmos. Chem. Phys., 18, 14623–14636, DOI:10.5194/acp-18-14623-2018, 2018.

De Graaf, M., L. G. Tilstra, P. Wang, and P. Stammes: Retrieval of the aerosol direct radiative effect over clouds from spaceborne spectrometry, J. Geophys. Res., 117, D07207, doi:10.1029/2011JD017160, 2012.

© Author(s) 2019. CC BY 4.0 License.

De Graaf, M., N. Bellouin, L. G. Tilstra, J. Haywood, and P. Stammes: Aerosol direct radiative effect of smoke over clouds over the southeast Atlantic Ocean from 2006 to 2009, Geophys. Res. Lett., 41, 7723-7730, doi:10.1002/2014GL061103, 2014.

Devasthale, A. and Thomas, M. A.: A global survey of aerosol-liquid water cloud overlap based on four years of CALIPSO-CALIOP data, Atmos. Chem. Phys., 11(3), 1143–1154, doi:10.5194/acp-11-1143-2011, 2011.

Dubovik, O., Holben, B., Eck, T. F., Smirnov, A., Kaufman, Y. J., King, M. D., Tanré, D. and Slutsker, I.: Variability of Absorption and Optical Properties of Key Aerosol Types Observed in Worldwide Locations, J. Atmos. Sci., 59(3), 590–608, doi:10.1175/1520-0469(2002)059<0590:VOAAOP>2.0.CO;2, 2002.

Dubovik, O. and King, M. D.: A flexible inversion algorithm for retrieval of aerosol optical properties from Sun and sky radiance measurements, J. Geophys. Res. Atmos., 105(D16), 20673–20696, doi:10.1029/2000JD900282, 2000.

Dunagan, S. E., Johnson, R., Zavaleta, J., Russell, P. B., Schmid, B., Flynn, C., Redemann, J., Shinozuka, Y., Livingston, J. and Segal-Rosenhaimer, M.: Spectrometer for Sky-Scanning Sun-Tracking Atmospheric Research (4STAR): Instrument technology, Remote Sens., 5(8), 3872–3895, doi:10.3390/rs5083872, 2013.

Eck, T., Holben, B. and Reid, J.: Wavelength dependence of the optical depth of biomass burning, urban, and desert dust aerosols,J. Geophys. Res. Atmos., 104(1), 31333–31349, doi: 10.1029/1999JD900923, 1999.

Eck, T. F., Holben, B. N., Ward, D. E., Mukelabai, M. M., Dubovik, O., Smirnov, A., Schafer, J. S., Hsu, N. C., Piketh, S. J., Queface, A., Roux, J. Le, Swap, R. J. and Slutsker, I.: Variability of biomass burning aerosol optical characteristics in southern Africa during the SAFARI 2000 dry season campaign and a comparison of single scattering albedo estimates from radiometric measurements, J. Geophys. Res. Atmos., 108(D13), 8477, doi:10.1029/2002JD002321, 2003.

Feng, N., and S. A. Christopher: Measurement-based estimates of direct radiative effects of absorbing aerosols above clouds, J. Geophys. Res. Atmos., 120, 6908–6921, doi:10.1002/2015JD023252, 2015.

Graßl, H.: Possible changes of planetary albedo due to aerosol particles, in Man's Impact on Climate, edited by: W. Bach, J. Pankrath, and W. Kellogg, Elsevier, New York, 1979.

Hobbs, P. V.: Clean air slots amid dense atmospheric pollution in southern Africa, J. Geophys. Res. Atmos., 108(D13), 8490, doi:10.1029/2002JD002156, 2003.

Holben, B. N., Eck, T. F., Slutsker, I., Tanre, D., Vermote, E., Reagan, J. A., Kaufman, Y. J., Nakajima, T., Lavenu, F., Jankowiak, I. and Smirnov, A.: AERONET — A Federated Instrument

© Author(s) 2019. CC BY 4.0 License.

Network and Data Archive for Aerosol Characterization, Remote Sens. Environ., 4257(98), 1998.

Holben, B. N., Kim, J., Sano, I., Mukai, S., Eck, T. F., Giles, D. M., Schafer, J. S., Sinyuk, A., Slutsker, I., Smirnov, A., Sorokin, M., Anderson, B. E., Che, H., Choi, M., Crawford, J. H., Ferrare, R. A., Garay, M. J., Jeong, U., Kim, M., Kim, W., Knox, N., Li, Z., Lim, H. S., Liu, Y., Maring, H., Nakata, M., Pickering, K. E., Piketh, S., Redemann, J., Reid, J. S., Salinas, S., Seo, S., Tan, F., Tripathi, S. N., Toon, O. B., and Xiao, Q.: An overview of mesoscale aerosol processes, comparisons, and validation studies from DRAGON networks, Atmos. Chem. Phys., 18, 655-671, https://doi.org/10.5194/acp-18-655-2018, 2018.

Howell, S. G., Clarke, A. D., Shinozuka, Y., Kapustin, V., McNaughton, C. S., Huebert, B. J., Doherty, S. J. and Anderson, T. L.: Influence of relative humidity upon pollution and dust during ACE-Asia: Size distributions and implications for optical properties, J. Geophys. Res. Atmos., 111(6), 1–11, doi:10.1029/2004JD005759, 2006.

Jethva, H., O. Torres, L. A. Remer, and P. K. Bhartia: A color ratio method for simultaneous retrieval of aerosol and cloud optical thickness of above-cloud absorbing aerosols from passive sensors: Application to MODIS measurements, IEEE Trans. Geosci. Remote Sens., 51(7), 3862-3870, doi:10.1109/TGRS.2012.2230008, 2013.

Jethva, H., O. Torres, F. Waquet, D. Chand, and Y. Hu: How do A-train sensors intercompare in the retrieval of above cloud aerosol optical depth? A case study-based assessment, Geophys. Res. Lett., 41, doi:10.1002/2013GL058405, 2014.

Kacenelenbogen M. et al, Global aerosol optical depths, extinction-to-backscatter (lidar) ratios and shortwave direct radiative effect above opaque water clouds, using primarily level 1 products from CALIOP/ CALIPSO, JGR, in preparation

Kaskaoutis, D. G. and Kambezidis, H. D.: Comparison of the Ångström parameters retrieval in different spectral ranges with the use of different techniques, Meteorol. Atmos. Phys., 99, 233–246, doi:10.1007/s00703-007-0279-y, 2008.

Keil, A. and Haywood, J. M.: Solar radiative forcing by biomass burning aerosol particles during SAFARI 2000: A case study based on measured aerosol and cloud properties, J. Geophys. Res. Atmos., 108(D13), n/a-n/a, doi:10.1029/2002JD002315, 2003.

Lack, D. A. and Cappa, C. D.: Impact of brown and clear carbon on light absorption enhancement, single scatter albedo and absorption wavelength dependence of black carbon, Atmos. Chem. Phys., 10(9), 4207–4220, doi:10.5194/acp-10-4207-2010, 2010.

LeBlanc, S. E., Schmidt, K. S., Pilewskie, P., Redemann, J., Hostetler, C., Ferrare, R., Hair, J., Langridge, J. M. and Lack, D. a.: Spectral aerosol direct radiative forcing from airborne radiative

© Author(s) 2019. CC BY 4.0 License.

measurements during CalNex and ARCTAS, J. Geophys. Res., 117, D00V20, doi:10.1029/2012JD018106, 2012.

LeBlanc, S. E.: samuelleblanc/fp: Moving Lines: NASA airborne research flight planning tool release, doi:10.5281/zenodo.1478126, 2018.

Levy, R. C., Mattoo, S., Munchak, L. A., Remer, L. A., Sayer, A. M., Patadia, F. and Hsu, N. C.: The Collection 6 MODIS aerosol products over land and ocean, Atmos. Meas. Tech., 6(11), 2989–3034, doi:10.5194/amt-6-2989-2013, 2013.

Liu, X., Huey, G., Yokelson, R. J., Selimovic, V., Simpson, I., Müller, M., Jimenez, J., Campuzano-Jost, P., Beyersdorf, A., Blake, D., Butterfield, Z., Choi, Y., Crounse, J., Day, D., Diskin, G., Dubey, M., Fortner, E., Hanisco, T., Weiwei, H., King, L., Kleinman, L., Meinardi, S., Mikoviny, T., Onasch, T., Palm, B., Peischl, J., Pollack, I., Ryerson, T., Sachse, G., Sedlacek, A., Shilling, J., Springston, S., St. Clair, J., Tanner, D., Teng, A., Wennberg, P., Wisthaler, A. and Wolfe, G.: Airborne measurements of western U.S. wildfire emissions: Comparison with prescribed burning and air quality implications, J. Geophys. Res. Atmos., 122(11), 6108–6129, doi:10.1002/2016JD026315, 2017.

Lohmann, U. and Feichter, J.: Global indirect aerosol effects: a review, Atmos. Chem. Phys., 5(3), 715–737, 2005.

Matus, Alexander V., et al.: The role of clouds in modulating global aerosol direct radiative effects in spaceborne active observations and the Community Earth System Model." Journal of Climate 28.8: 2986-3003, 2015.

McGill, M. J., Yorks, J. E., Scott, V. S., Kupchock, A. W., and P. A. S.: The Cloud-Aerosol Transport System (CATS): a technology demonstration on the International Space Station, Proc.SPIE, 9612, 9612-9612–6, doi:10.1117/12.2190841, 2015.

Mcnaughton, C. S., Clarke, A. D., Howell, S. G., Anderson, B., Thornhill, L., Hudgins, C., Dibb, J. E., Scheuer, E., Maring, H., Mcnaughton, C. S., Clarke, A. D., Howell, S. G., Anderson, B., Thornhill, L., Hudgins, C., Winstead, E., Dibb, J. E., Mcnaughton, C. S., Clarke, A. D., Howell, S. G., Pinkerton, M., Anderson, B., Thornhill, L., Hudgins, C., Winstead, E., Dibb, J. E., Scheuer, E. and Maring, H.: Results from the DC-8 Inlet Characterization Experiment (DICE): Airborne Versus Surface Sampling of Mineral Dust and Sea Salt Aerosols Results from the DC-8 Inlet Characterization Experiment (DICE): Airborne Versus Surface Sampling of Mineral Dust and, Aerosol Sci. Technol., 6826, 41:136-159, doi:10.1080/02786820601118406, 2007.

Meyer, K., Platnick, S. and Zhang, Z.: Simultaneously inferring above-cloud absorbing aerosol optical thickness and underlying liquid phase cloud optical and microphysical properties using MODIS, J. Geophys. Res. Atmos., 120, 5524-5547, doi:10.1002/2015JD023128, 2015.

O'Neill, N.T., T.F.Eck, B.N.Holben, A.Smirnov, O.Dubovik, and A.Royer: Bimodal size distribution influences on the variation of Angstrom derivatives in spectral and optical depth space, J. Geophys. Res., 106, 9787-9806, 2001.

© Author(s) 2019. CC BY 4.0 License.

O'Neill, N. T., Eck, T. F., Smirnov, a, Holben, B. N. and Thulasiraman, S.: Spectral discrimination of coarse and fine mode optical depth, J. Geophys. Res., 108(D17), 4559, doi:10.1029/2002JD002975, 2003.

ORACLES Science Team: Suite of Aerosol, Cloud, and Related Data Acquired Aboard P3 During ORACLES 2016, Version 1, NASA Ames Earth Science Project Office, doi:10.5067/Suborbital/ORACLES/P3/2016_V1, 2017.

Peers, F., Waquet, F., Cornet, C., Dubuisson, P., Ducos, F., Goloub, P., Szczap, F., Tanré, D., and Thieuleux, F.: Absorption of aerosols above clouds from POLDER/PARASOL measurements and estimation of their direct radiative effect, Atmos. Chem. Phys., 15, 4179-4196, https://doi.org/10.5194/acp-15-4179-2015, 2015.

Platnick, S., Meyer, K. G., King, M. D., Wind, G., Amarasinghe, N., Marchant, B., Arnold, G. T., Zhang, Z., Hubanks, P. A., Holz, R. E., Yang, P., Ridgway, W. L. and Riedi, J.: The MODIS Cloud Optical and Microphysical Products: Collection 6 Updates and Examples From Terra and Aqua, IEEE Trans. Geosci. Remote Sens., 55(1), 502–525, doi:10.1109/TGRS.2016.2610522, 2017.

Pósfai, M., Simonics, R., Li, J., Hobbs, P. V. and Buseck, P. R.: Individual aerosol particles from biomass burning in southern Africa: 1. Compositions and size distributions of carbonaceous particles, J. Geophys. Res. Atmos., 108(D13), 8483, doi:10.1029/2002JD002291, 2003.

Provencal, R., Gupta, M., Owano, T. G., Baer, D. S., Ricci, K. N., O'Keefe, A. and Podolske, J. R.: Cavity-enhanced quantum-cascade laser-based instrument for carbon monoxide measurements, Appl. Opt., 44(31), 6712–6717, doi:10.1364/AO.44.006712, 2005.

Quinn, P. K., Bates, T. S., Baynard, T., Clarke, A. D., Onasch, T. B., Wang, W., Rood, M. J., Andrews, E., Allan, J., Carrico, C. M., Coffman, D. and Worsnop, D.: Impact of particulate organic matter on the relative humidity dependence of light scattering: A simplified parameterization, Geophys. Res. Lett., 32, 3–6, doi:10.1029/2005GL024322, 2005.

Rajapakshe, C., Zhang, Z., Yorks, J. E., Yu, H., Tan, Q., Meyer, K., Platnick, S. and Winker, D. M.: Seasonally transported aerosol layers over southeast Atlantic are closer to underlying clouds than previously reported, Geophys. Res. Lett., 44(11), 5818–5825, doi:10.1002/2017GL073559, 2017.

Russell, P. B., Bergstrom, R. W., Shinozuka, Y., Clarke, a D., DeCarlo, P. F., Jimenez, J. L., Livingston, J. M., Redemann, J., Dubovik, O. and Strawa, A.: Absorption Angstrom Exponent in AERONET and related data as an indicator of aerosol composition, Atmos. Chem. Phys., 10(3), 1155–1169, 2010.

© Author(s) 2019. CC BY 4.0 License.

Russell, P. B., Kacenelenbogen, M., Livingston, J. M., Hasekamp, O. P., Redemann, J., Ramachandran, S., Holben, B. and Al, R. E. T.: A multiparameter aerosol classification method and its application to retrievals from spaceborne polarimetry, J. Geophys. Res. Atmos., 119, 9838–9863, doi:10.1002/2013JD021411, 2014.

Sakaeda, N., Wood, R. and Rasch, P. J.: Direct and semidirect aerosol effects of southern African biomass burning aerosol, J. Geophys. Res. Atmos., 116(12), 1–19, doi:10.1029/2010JD015540, 2011.

Sayer, A. M., A. Smirnov, N. C. Hsu, and B. N. Holben, A pure marine aerosol model, for use in remote sensing applications, J. Geophys. Res., 117, D05213, doi:10.1029/2011JD016689, 2012.

Sayer, A. M., Hsu, N. C., Bettenhausen, C., Lee, J., Redemann, J., Schmid, B. and Shinozuka, Y.: Extending "Deep Blue" aerosol retrieval coverage to cases of absorbing aerosols above clouds : Sensitivity analysis and first case studies, J. Geophys. Res. Atmos., 121, 4830–4854, doi:10.1002/2015JD024729, 2016.

Schmid, B. and Wehrli, C.: Comparison of sun photometer calibration by Langley technique and standard lamp, Appl. Optics, 34, 4500–4512, 1995.

Schulz, M., Textor, C., Kinne, S., Balkanski, Y., Bauer, S., Berntsen, T., Berglen, T., Boucher, O., Dentener, F., Guibert, S., Isaksen, I. S. a., Iversen, T., Koch, D., Kirkevåg, A., Liu, X., Montanaro, V., Myhre, G., Penner, J. E., Pitari, G., Reddy, S., Seland, Ø., Stier, P. and Takemura, T.: Radiative forcing by aerosols as derived from the AeroCom present-day and pre-industrial simulations, Atmos. Chem. Phys., 6, 5225–5246, doi:10.5194/acpd-6-5095-2006, 2006.

Segal-Rosenheimer, M., et al.: Tracking elevated pollution layers with a newly developed hyperspectral Sun/Sky spectrometer (4STAR): Results from the TCAP 2012 and 2013 campaigns, J. Geophys. Res. Atmos., 119, doi:10.1002/2013JD020884, 2014.

Shinozuka, Y., Redemann, J., Livingston, J. M., Russell, P. B., Clarke, A. D., Howell, S. G., Freitag, S., O'Neill, N. T., Reid, E. A., Johnson, R., Ramachandran, S., McNaughton, C. S., Kapustin, V. N., Brekhovskikh, V., Holben, B. N., and McArthur, L. J. B.: Airborne observation of aerosol optical depth during ARCTAS: vertical profiles, inter-comparison and fine-mode fraction, Atmos. Chem. Phys., 11, 3673-3688, https://doi.org/10.5194/acp-11-3673-2011, 2011.

Small, J. D., Chuang, P. Y., Feingold, G. and Jiang, H.: Can aerosol decrease cloud lifetime?, Geophys. Res. Lett., 36(16), 1–5, doi:10.1029/2009GL038888, 2009.

Torres, O., J. Hiren, and P. K. Bhartia: Retrieval of aerosol optical depth above clouds from OMI observations: Sensitivity analysis and case studies. J. Atmos. Sci., 69, 1037-1053, 2012.

© Author(s) 2019. CC BY 4.0 License.

Twomey, S. A.: Pollution and the planetary albedo, Atmos. Environ., 8, 1251–1256, 1974.

Twomey, S.: The influence of pollution on the shortwave albedo of clouds, J. Atmos. Sci., 34, 1149–1152, 1977.

Waquet F., J. Riedi, L. C. Labonnote, P. Goloub, B. Cairns, J-L. Deuzé, and D. Tanré: Aerosol Remote Sensing over Clouds Using A-Train Observations. J. Atmos. Sci., 66, 2468-2480, 2009.

Waquet, F., Peers, F., Ducos, F., Goloub, P, Platnick, S., Riedi, J., Tanré, D., Thieuleux, F.: Global analysis of aerosol properties above clouds. Geophysical Research Letters. 40. 5809-5814. 10.1002/2013GL057482, 2013a.

Waquet, F., et al.: Retrieval of aerosol microphysical and optical properties above liquid clouds from POLDER/PARASOL polarization measurements, Atmos. Meas. Tech., 6, 991-1016, doi:10.5194/amt-6-991, 2013b.

Wilcox, E. M.: Direct and semi-direct radiative forcing of smoke aerosols over clouds, Atmos. Chem. Phys., 12, 139-149, doi:10.5194/acp-12-139-2012, 2012.

Wood et al.,: Observations of Aerosols above Clouds and their interactions (ORACLES): science questions, background and summary of the 2016 field deployment, In Preparation for Atmos. Chem. Phys.

Yoon, J., Von Hoyningen-Huene, W., Kokhanovsky, A. A., Vountas, M. and Burrows, J. P.: Trend analysis of aerosol optical thickness and Ångström exponent derived from the global AERONET spectral observations, Atmos. Meas. Tech., 5(6), 1271–1299, doi:10.5194/amt-5-1271-2012, 2012.

Zhang, Z., K. Meyer, S. Platnick, L. Oreopoulos, D. Lee, and H. Yu: A novel method for estimating shortwave direct radiative effect of above-cloud aerosols using CALIOP and MODIS data, Atmos Meas Tech, 7(6), 1777-1789, doi:10.5194/amt-7-1777-2014, 2014.

Zhang, Z., Meyer, K., Yu, H., Platnick, S., Colarco, P., Liu, Z. and Oreopoulos, L.: Shortwave direct radiative effects of above-cloud aerosols over global oceans derived from 8 years of CALIOP and MODIS observations, Atmos. Chem. Phys., 16(5), 2877–2900, doi:10.5194/acp-16-2877-2016, 2016.

Zuidema, P., Redemann, J., Haywood, J., Wood, R., Piketh, S., Hipondoka, M. and Formenti, P.: Smoke and clouds above the southeast Atlantic: Upcoming field campaigns probe absorbing aerosol's impact on climate, Bull. Am. Meteorol. Soc., 97(7), 1131–1135, doi:10.1175/BAMS-D-15-00082.1, 2016

Atmos. Chem. Phys. Discuss., https://doi.org/10.5194/acp-2019-43
Manuscript under review for journal Atmos. Chem. Phys.
Discussion started: 30 January 2019
© Author(s) 2019. CC BY 4.0 License.

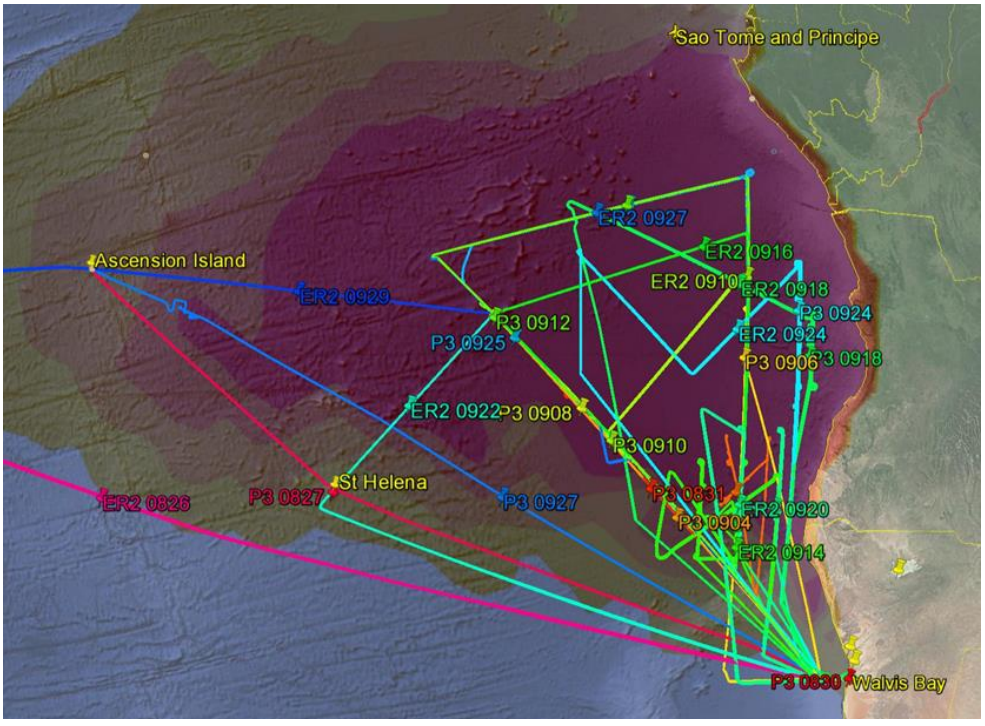

Figure 1 – Map (from Google earth) of the South-East Atlantic (SEA) region with flight paths from the NASA P-3B and the NASA ER-2 during ORACLES deployment of 2016. Climatological aerosol optical depth from MODIS for September (2001-2013) is overlaid as colored shaded contours (yellow shading represents AOD of 0.25, with deep red shading for 0.5 (adapted from Zuidema et al., 2016)).

Atmos. Chem. Phys. Discuss., https://doi.org/10.5194/acp-2019-43
Manuscript under review for journal Atmos. Chem. Phys.
Discussion started: 30 January 2019
© Author(s) 2019. CC BY 4.0 License.

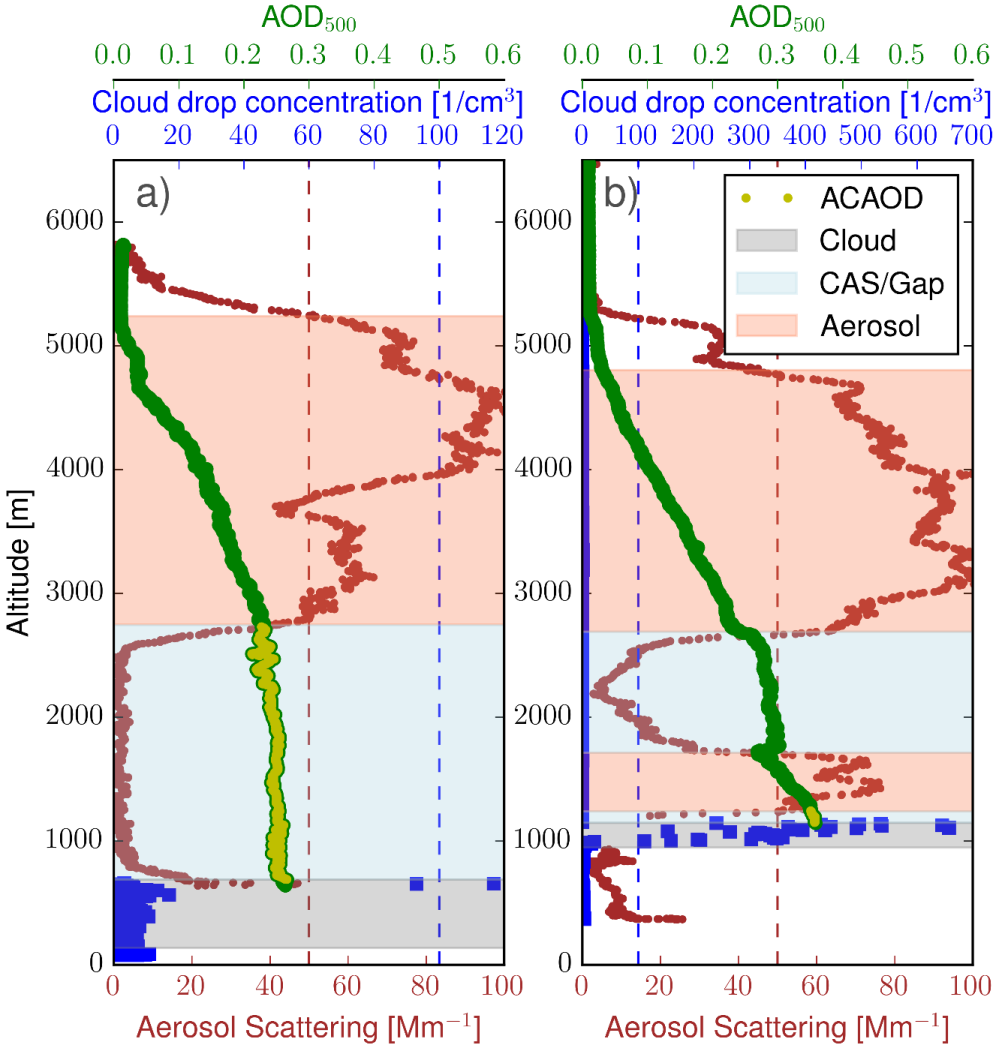

Figure 2 - Examples of profiles of cloud drop concentration from PDI, aerosol scattering (at 550 nm) from HiGEAR's nephelometer, and AOD measurements used to evaluate the ACAOD portion of the total AOD column taken from flight on 2016-09-12. a) case from 18.6°S, 8.6°E where there is a gap (light blue shading) between cloud top (grey shading) and an aerosol layer (light red shading). The yellow markers within the green AOD profile denotes the vertical portion of the flight representing the ACAOD. b) case from 10.2°S, 0.2°E with a near zero separation between cloud top and aerosol layer, but with an embedded gap within the aerosol layer. For this case, only the AOD directly above cloud is considered ACAOD.

Atmos. Chem. Phys. Discuss., https://doi.org/10.5194/acp-2019-43
Manuscript under review for journal Atmos. Chem. Phys.
Discussion started: 30 January 2019
© Author(s) 2019. CC BY 4.0 License.

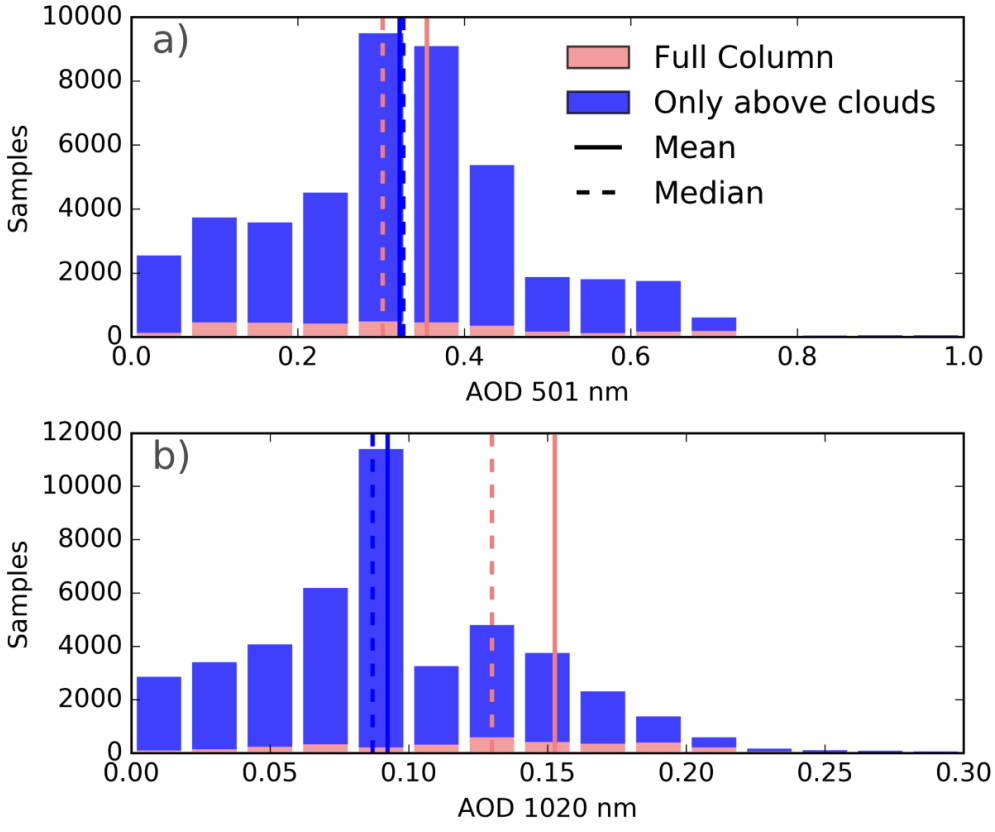

Figure 3 - Histograms of above-cloud (blue) and full-column (pink) AOD sampled by 4STAR at (a) 501 nm and (b) 1020 nm. 'Full column' denotes sampling below an altitude of 0.6 km where no cloud is between 4STAR and the sun (N=3,388), while 'Only above clouds' denotes the AOD flagged to be only above clouds (see Sect. 2.6, N=41,189). Vertical solid lines denote the mean of the distribution (colored accordingly), while dashed vertical lines denote the median.

Atmos. Chem. Phys. Discuss., https://doi.org/10.5194/acp-2019-43
Manuscript under review for journal Atmos. Chem. Phys.
Discussion started: 30 January 2019
© Author(s) 2019. CC BY 4.0 License.

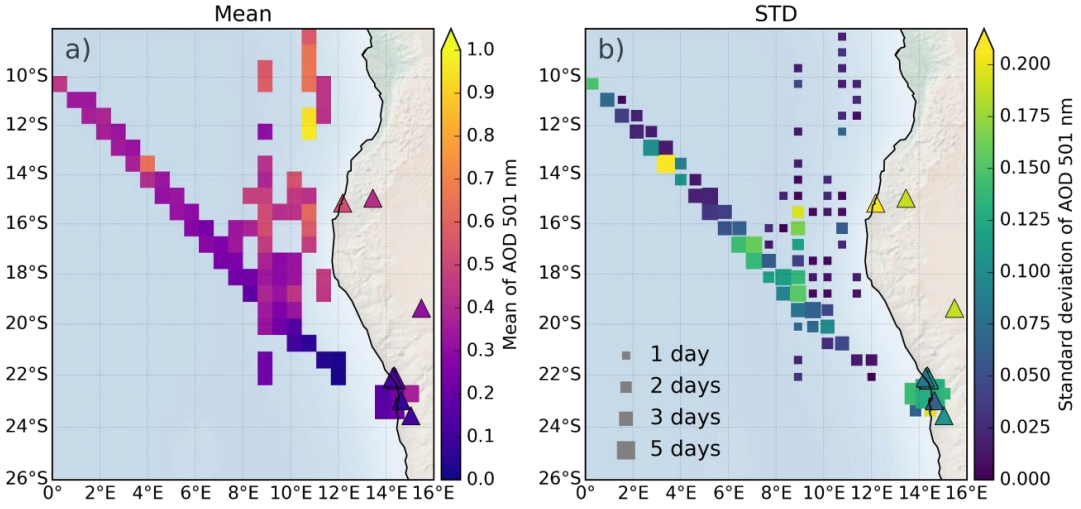

Figure 4 - (a): Map of mean $ACAOD_{501}$ from all P-3 flights spatially binned during ORACLES 2016 deployment period. The triangles indicate the location of the ground based AERONET stations, colored by their average full column fine mode AOD_{501}. (b): the standard deviation of $ACAOD_{501}$ within each bin with the size of the squares denoting the number of days sampled within each bin. The legend in the bottom left of the panel denotes the different sizes of the square symbol relating to the number of sampled days in each bin. The triangles indicate the standard deviation of the fine mode AOD measured by the ground based AERONET stations from north to south: Lubango, Namibe, DRAGON network at Henties Bay, Walvis Bay Airport, and Gobabeb.

Atmos. Chem. Phys. Discuss., https://doi.org/10.5194/acp-2019-43
Manuscript under review for journal Atmos. Chem. Phys.
Discussion started: 30 January 2019
© Author(s) 2019. CC BY 4.0 License.

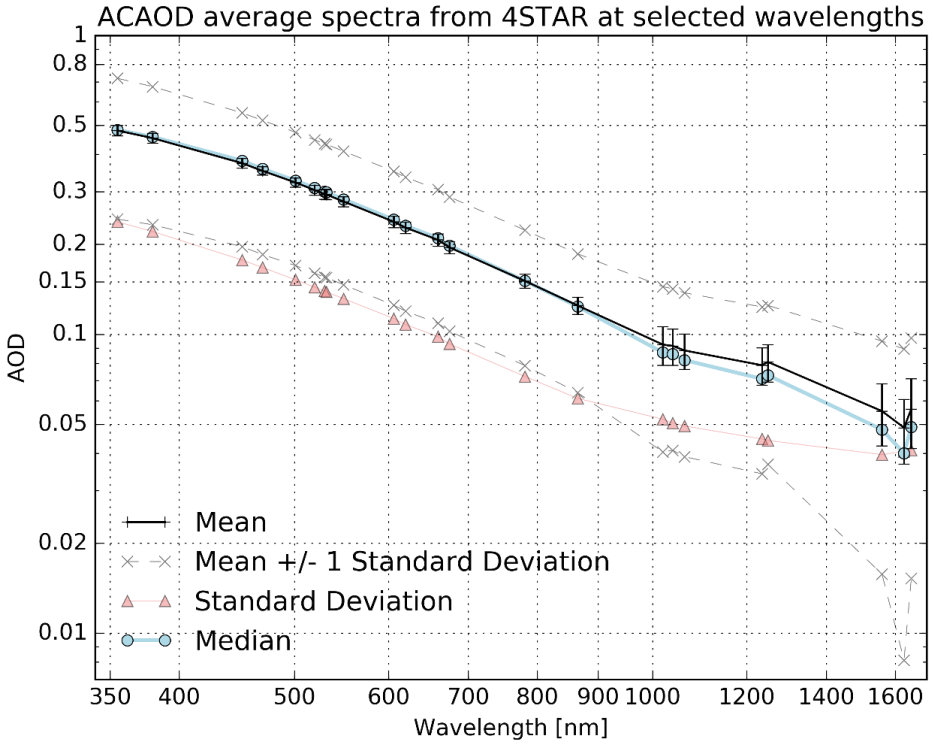

Figure 5 - ACAOD spectra representing the mean, median, and standard deviation of measurements by 4STAR for selected wavelengths, which have minimal influence of gas absorption and high signal to noise ratio. The mean measured ACAOD at each wavelength is shown in black, along with its mean uncertainty (as error bars in black), median in blue circles, and the range of 1 standard deviation surrounding the mean for all the measured ACAOD (grey dashed lines). The magnitude of the standard deviation is also included, denoted by a thin pink line with triangles.

Atmos. Chem. Phys. Discuss., https://doi.org/10.5194/acp-2019-43
Manuscript under review for journal Atmos. Chem. Phys.
Discussion started: 30 January 2019
© Author(s) 2019. CC BY 4.0 License.

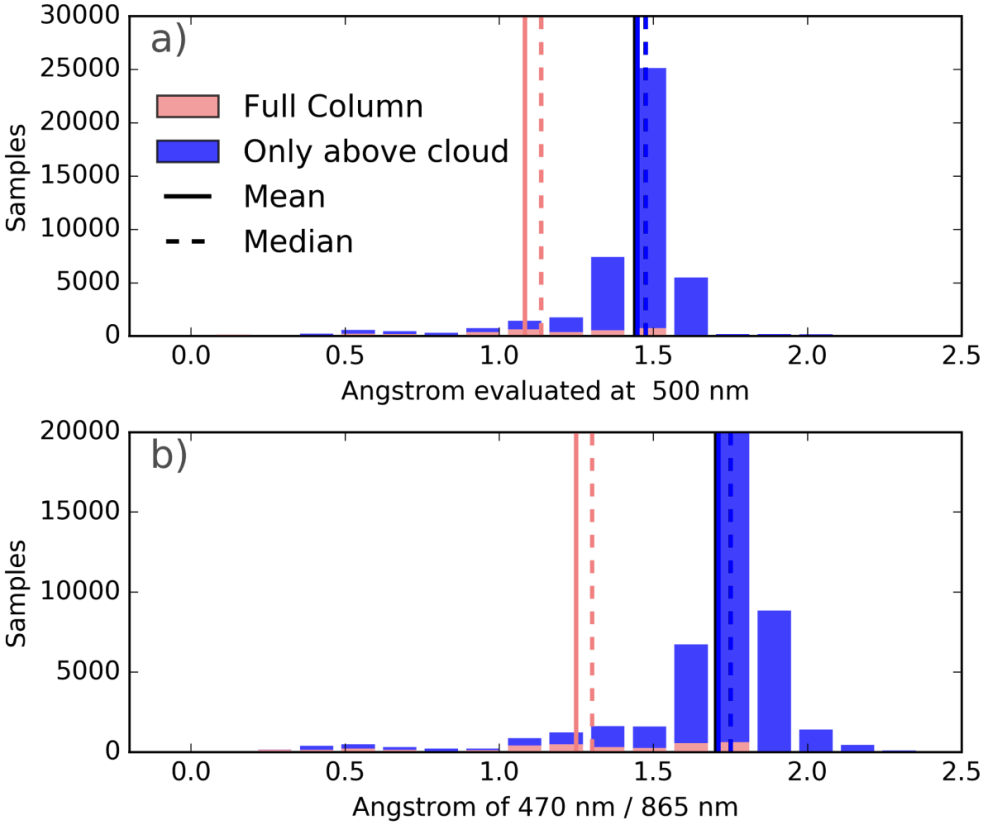

Figure 6 - Histograms of Ångström exponent (AE) calculated from (a) a polynomial fit of AOD sampled by 4STAR evaluated at 500 nm and (b) using the 2-wavelength ratio (470 nm and 865 nm) in log-normal space, for the full column AOD (pink) and the ACAOD (blue).

5

Atmos. Chem. Phys. Discuss., https://doi.org/10.5194/acp-2019-43
Manuscript under review for journal Atmos. Chem. Phys.
Discussion started: 30 January 2019
© Author(s) 2019. CC BY 4.0 License.

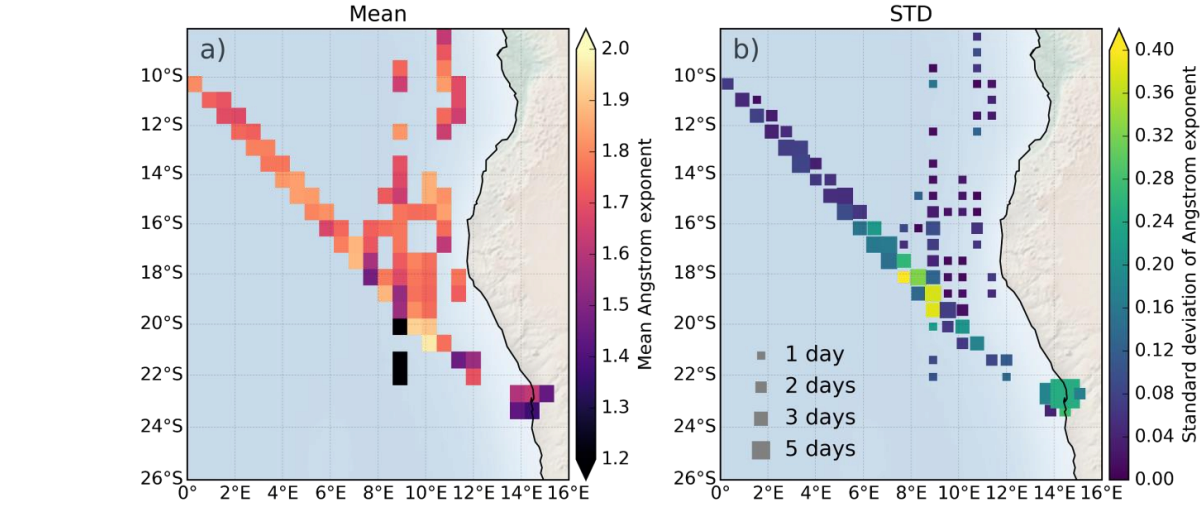

Figure 7 - Map of mean AE derived from AOD spectra of aerosols above clouds calculated from two wavelengths (470/865 nm) (a), and the standard deviation of the AE (b), where the size of the squares represents the number of sampling days used to build the statistics within each gridded bins.

5

Atmos. Chem. Phys. Discuss., https://doi.org/10.5194/acp-2019-43
Manuscript under review for journal Atmos. Chem. Phys.
Discussion started: 30 January 2019
© Author(s) 2019. CC BY 4.0 License.

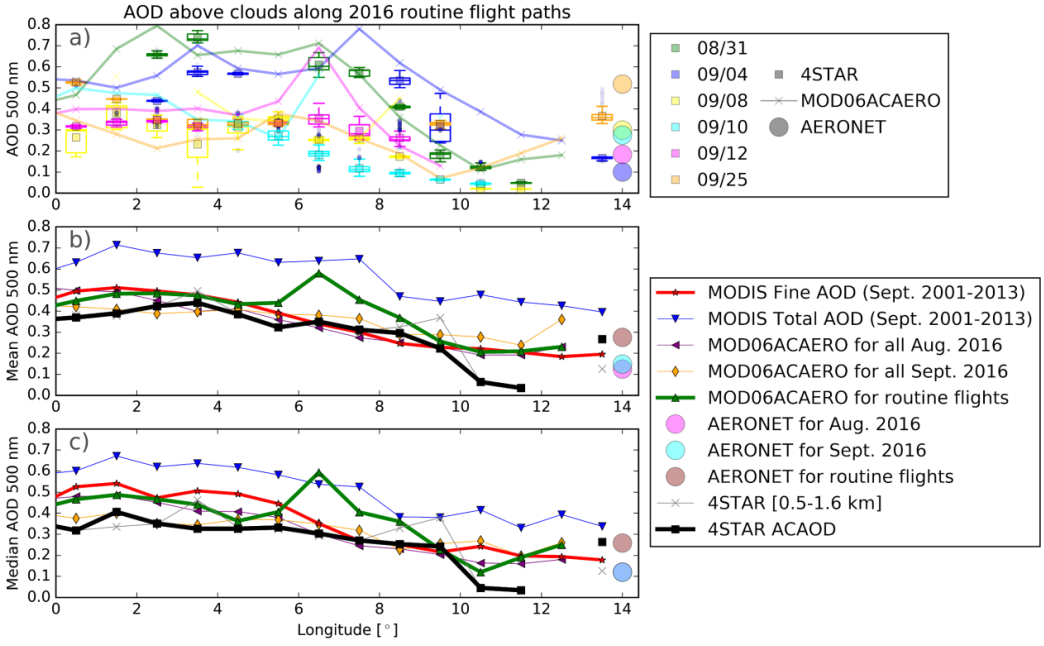

Figure 8 - ACAOD at 501 nm along the diagonal routine flight path (13°E 23°S to 0°E 10°S) for ORACLES 2016 compared to a MODIS climatology, MOD06ACAERO (Aerosol Above Cloud retrieved from MODIS satellites (Meyer et al., 2015)) retrievals as a function of longitude, and nearby ground based AERONET fine mode AOD. (a) The 4STAR ACAOD sampled during the days when the NASA P-3 followed the routine flight path and its equivalent retrievals from MOD06ACAERO. The 4STAR ACAOD is represented by box whisker plots, for binned longitudes, whereas the MODIS AAC is represented by its mean value within a longitude by an 'x' and connecting line. The AERONET fine mode AOD measured from DRAGON at Henties Bay, Namibia for the same days are presented in the far right as circles. (b) The mean of the ACAOD sampled over the days listed in the top panel for 4STAR and MOD06ACAERO compared to other retrieved measurements over a longer time period. The monthly mean MOD06ACAERO for August and September 2016, along with the clear sky mean total and fine mode AOD from MODIS from September averaged over the years 2001 - 2013. The mean AOD from 4STAR sampled within the altitude range of 0.5 - 1.6 km. (c) Median ACAOD instead of mean.

Atmos. Chem. Phys. Discuss., https://doi.org/10.5194/acp-2019-43
Manuscript under review for journal Atmos. Chem. Phys.
Discussion started: 30 January 2019
© Author(s) 2019. CC BY 4.0 License.

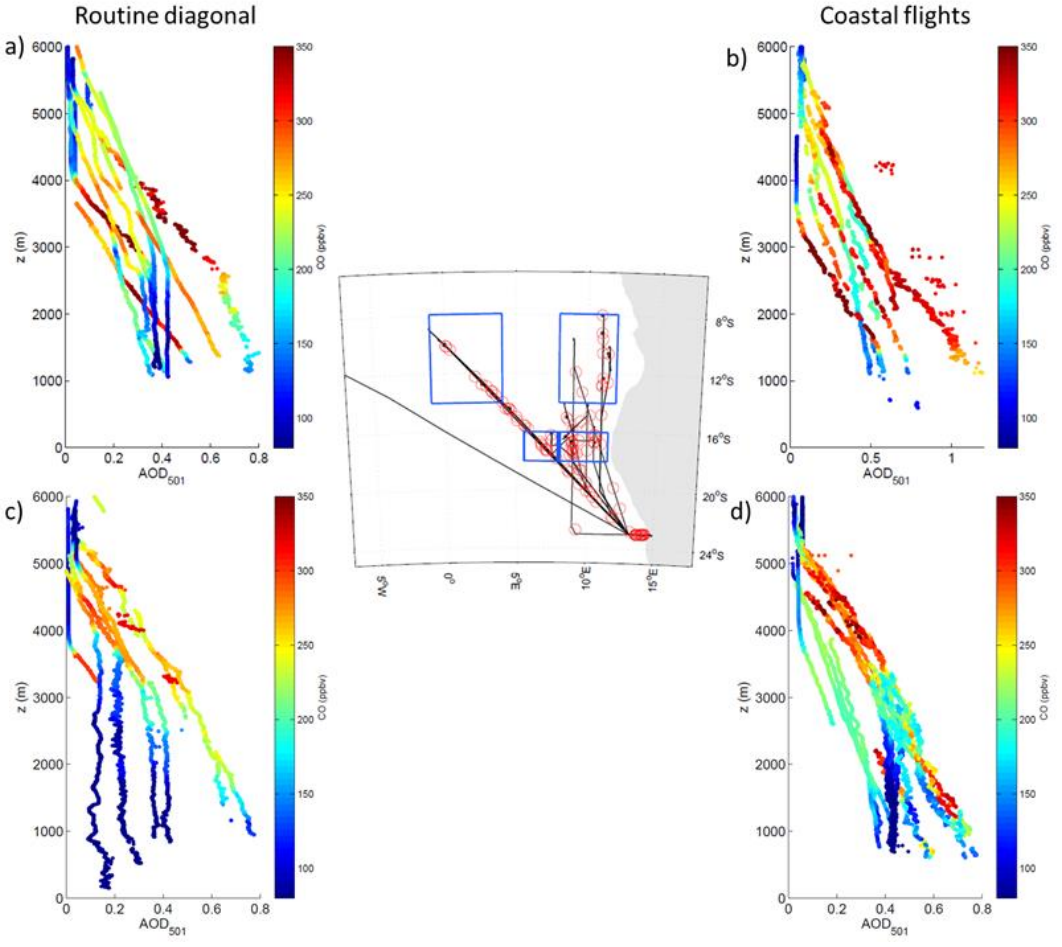

Figure 9 - A subset of AOD at 501 nm vertical profiles along the routine diagonal (left) and near the African coast (right) at the northernmost edge of the flight tracks (top; 8 to 14S) and near the bottom edge of the plume (bottom; 16 to 18S). Note that only a subset of profiles, roughly equal for each area, are shown for clarity of interpretation, though the middle-latitude profiles generally exhibit features of both latitude bins shown. Color indicates the CO concentration of the ambient airmass, measured by the in situ COMA instrument. The aerosol-cloud vertical gap is most prominent farther from the coast, as indicated by altitudes where low CO values are measured simultaneously with a low vertical gradient in AOD. Flights near the coast show more variability, and fewer cases of an unpolluted gap above cloud (greater low-level CO and stronger gradient of AOD with altitude), although each condition is seen within both regions. The central map shows the location of the subsets overlaid by all flight paths from ORACLES-2016 (black lines), and all P-3 aircraft profiles (red circles).

Atmos. Chem. Phys. Discuss., https://doi.org/10.5194/acp-2019-43
Manuscript under review for journal Atmos. Chem. Phys.
Discussion started: 30 January 2019
© Author(s) 2019. CC BY 4.0 License.

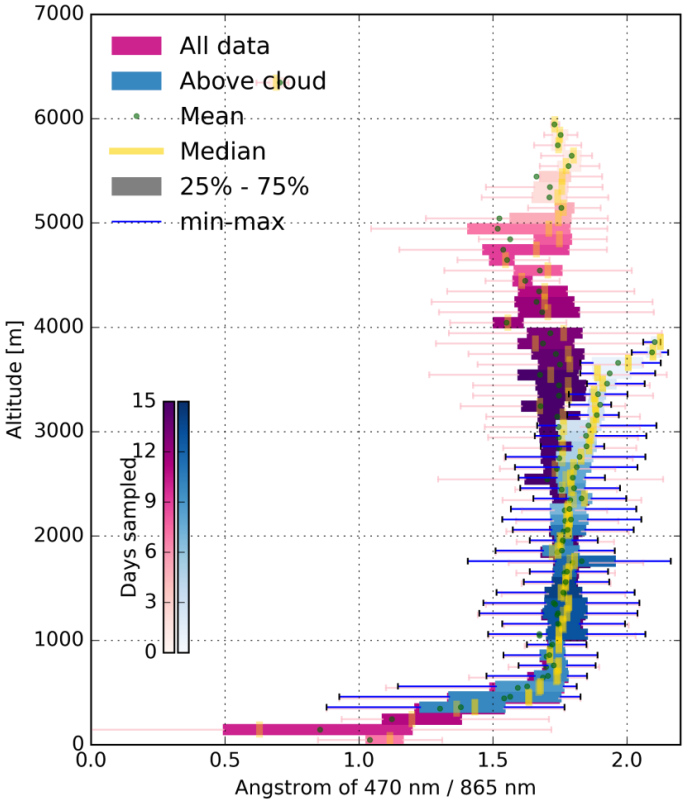

Figure 10 - Binned vertical profile of $AE_{470/865}$ for all measured AOD greater than 0.1, including all data (red-purple colors) and aerosol above cloud (blue colors). These represent the $AE_{470/865}$ calculated from all AOD spectra representing the aerosol above that altitude, and binned by 100 meters. The mean of each binned vertical population is represented by the green circle, median by the gold vertical line, the thick horizontal line represents the span of $AE_{470/865}$ from the 25th to the 75th percentile, while the range is denoted by the span of the thin blue (or pink) line. The shading of each box-and-whisker plot denote the amount of days sampled within this altitude bin, linked to the colorbars on the left side.

Atmos. Chem. Phys. Discuss., https://doi.org/10.5194/acp-2019-43
Manuscript under review for journal Atmos. Chem. Phys.
Discussion started: 30 January 2019
© Author(s) 2019. CC BY 4.0 License.

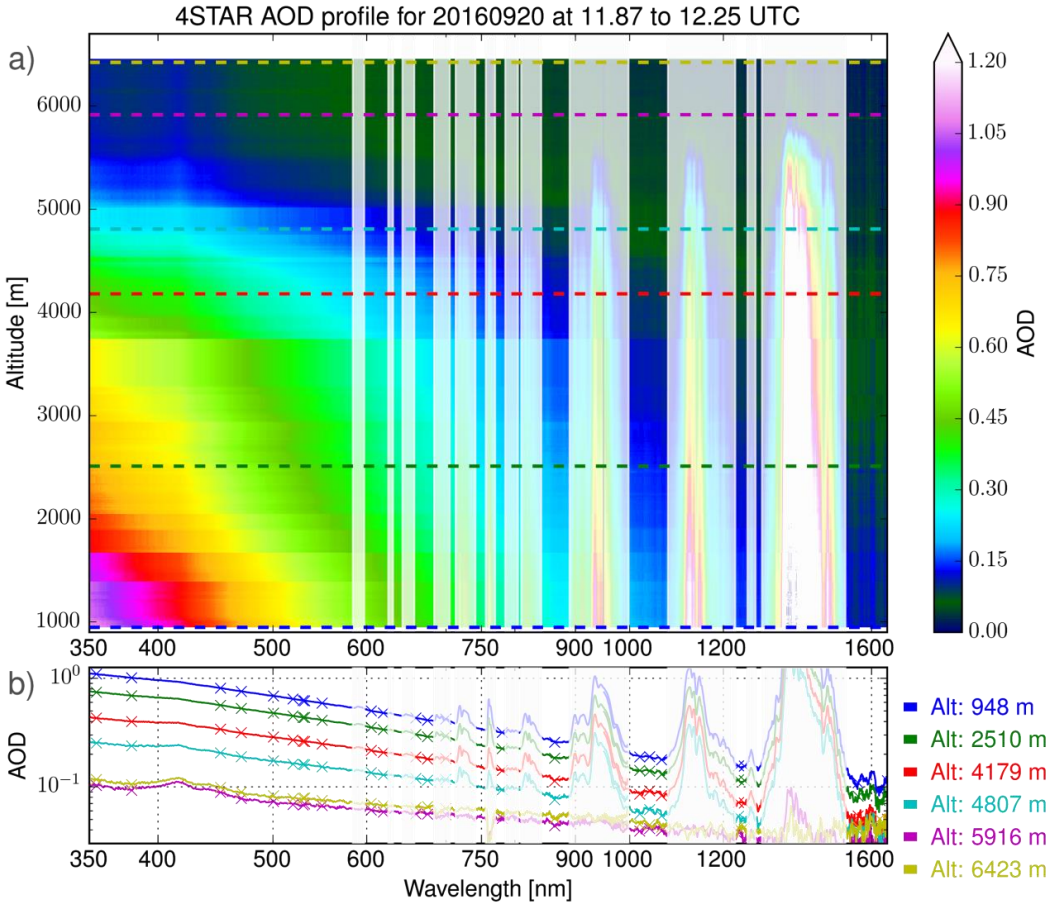

Figure 11 - Hyperspectral AOD profile from 20 September 2018, from a square spiral at 11:52 to 12:15 UTC. a) shows the AOD as the color (linked to the colorbar at the far right) continuously and as a function of wavelength and altitude. The shaded regions denote where strong gas absorbers, namely water vapor and oxygen impact the spectra. b) hyperspectral AOD at select altitudes, denoted by the dashed lines in a). The 'x' symbols denote the particular wavelengths at which the AOD is available in the ORACLES data archive, matching some wavelengths used by other instruments, and which the AOD is of highest confidence.

Atmos. Chem. Phys. Discuss., https://doi.org/10.5194/acp-2019-43
Manuscript under review for journal Atmos. Chem. Phys.
Discussion started: 30 January 2019
© Author(s) 2019. CC BY 4.0 License.

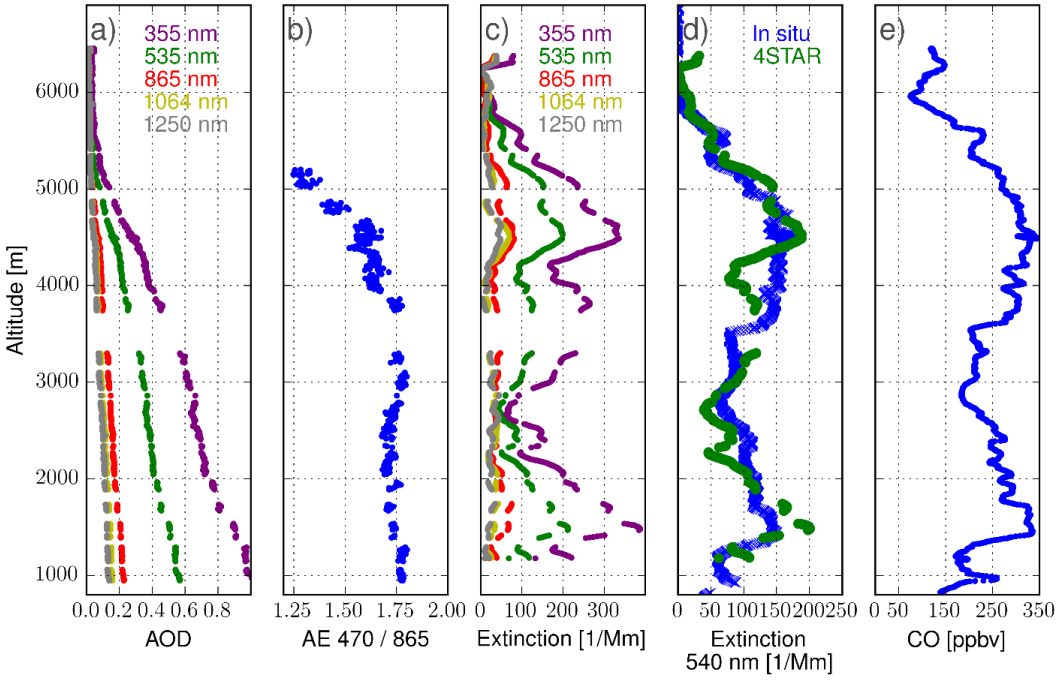

Figure 12 – Aerosol optical properties profiles from the same case on 2016-09-20 as fig. 11. (a) Vertical profile of AOD at a few selected wavelengths. (b) $AE_{470/865}$ profile, (c) derived extinction coefficient from 4STAR AOD at a few wavelengths, (d) extinction coefficient at 540 nm derived from 4STAR AOD and in situ measurements, (e) and CO concentration.

Atmos. Chem. Phys. Discuss., https://doi.org/10.5194/acp-2019-43
Manuscript under review for journal Atmos. Chem. Phys.
Discussion started: 30 January 2019
© Author(s) 2019. CC BY 4.0 License.

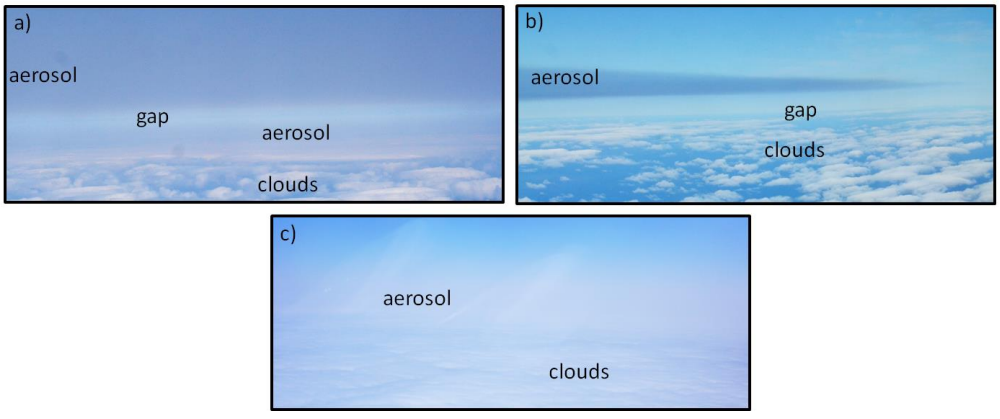

Figure 13 - Photographs taken from the P-3 of (a) a gap between two aerosol layers, (b) a gap between an aerosol layer and cloud, and (c) no gap between aerosol and cloud.

Atmos. Chem. Phys. Discuss., https://doi.org/10.5194/acp-2019-43
Manuscript under review for journal Atmos. Chem. Phys.
Discussion started: 30 January 2019
© Author(s) 2019. CC BY 4.0 License.

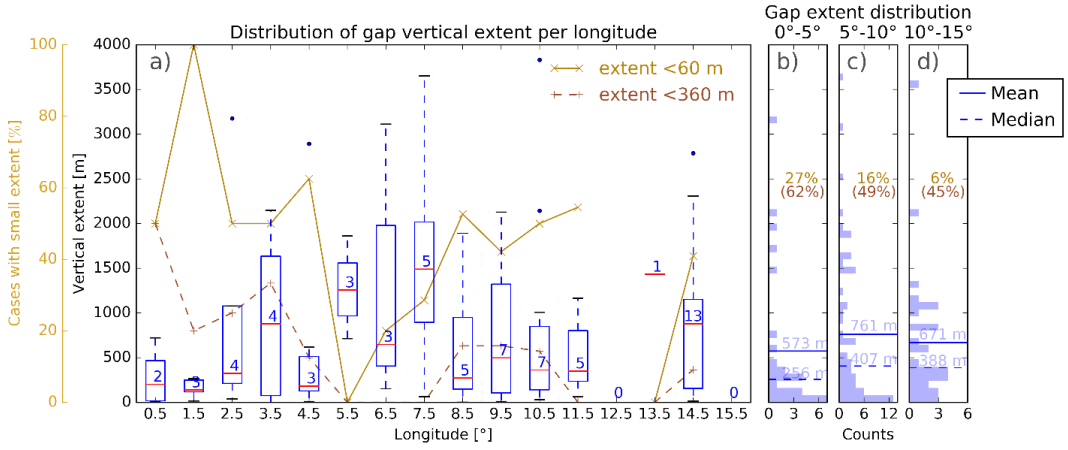

Figure 14 - Distribution of vertical extent where the AOD does not change significantly with changing altitude (cloud-aerosol gap). (a) Box-whisker plot (red line representing mean of the bin, box representing the interquartile range, whiskers representing the minimum and maximum range, and outliers represented by dots, which are further than 1.5 times the interquartile range from the first or third quartile) of the vertical extent binned by longitude. Numbers indicate the number of sampling days represented within each bin, with each day having more than one profile. The proportion of profiles/cases that are considered having a small extent is denoted by the gold and brown colors. (b, c, and d) The gap altitude distribution represented as a histogram for all sampled ACAOD from 4STAR for 3 separate longitudinal regions. The proportion of the gap extent that is near zero is indicated as a percentage in each panel (b, c, and d), the equivalent statistic for CEAL cases (within 360 m) is below in parentheses.

Atmos. Chem. Phys. Discuss., https://doi.org/10.5194/acp-2019-43
Manuscript under review for journal Atmos. Chem. Phys.
Discussion started: 30 January 2019
© Author(s) 2019. CC BY 4.0 License.

Atmospheric Chemistry and Physics Discussions

		All measurements			Spatially binned		
		mean	median	std	mean	median	std
ACAOD	501 nm	0.32	0.33	0.15	0.37	0.34	0.05
	1020 nm	0.09	0.09	0.05	0.11	0.09	0.02
Total Column AOD	501 nm	0.36	0.30	0.18	0.38	0.39	0.03
	1020 nm	0.15	0.13	0.06	0.15	0.14	0.04
ACAOD uncertainty	501 nm	0.011	0.01	0.008	0.013	0.011	0.004
	1020 nm	0.013	0.012	0.012	0.015	0.011	0.004
AE of ACAOD	470/865 nm	1.71	1.75	0.24	1.65	1.66	0.10
	500 nm	1.45	1.48	0.18	1.44	1.48	0.06
AE of Total Column	470/865 nm	1.25	1.30	0.46	1.23	1.33	0.09
	500 nm	1.08	1.14	0.37	1.07	1.19	0.07

Table 1 - Summary of measured aerosol optical properties during September 2016 as part of ORACLES.